CHAPTER 3 : Calculating geostrophic winds from sea level pressure data

Chapter authors:
G M Watson and Dr J A Halliday (CLRC Rutherford Appleton Laboratory) & Dr T Holt and Dr J P Palutikof (University of East Anglia)

3.1 Introduction

This Chapter describes in detail the first step in the POWER methodology (see Section 2.2) whereby mean sea level atmospheric pressure gradients are used to calculate geostrophic winds throughout an area of interest. It also reports on the application, testing and validation of this procedure in EU waters within the POWER project.

3.2 Theoretical background

The geostrophic wind is a theoretical wind calculated from surface pressure data. A balance is assumed between the flow of air from high to low pressure regions and the effects of the rotation of the Earth as manifested in the "Coriolis Effect". The geostrophic wind flows parallel to the isobars (contours of equal surface pressure), and a good approximation to the actual wind in the free atmosphere. A more detailed explanation of the geostrophic wind can be found in standard meteorological texts, for example, James (1994)

The geostrophic wind is the horizontal equilibrium wind (V_G), blowing parallel to the isobars, which represents the exact balance between the horizontal pressure gradient force:

$$-\left(1/\rho\right)\nabla_H p \qquad 3.1$$

and the horizontal component of the Coriolis Force:

$$fV_G \qquad 3.2$$

where $\nabla_H p$ is the horizontal pressure gradient, ρ is the air density, and f is the Coriolis parameter, which is a function of the Earth's angular momentum (Ω) and latitude (φ):

$$f = 2\Omega \sin\varphi . \qquad 3.3$$

The magnitude of V_G is given by:

$$V_G = \left|\left(1/f\rho\right)\nabla_H p\right| \qquad 3.4$$

Low pressure is to the left of the wind vector in the northern hemisphere, and to the right in the southern hemisphere.

From Equation 3.4, the geostrophic wind speed is a function of latitude, pressure gradient and air density. A reasonable assumption for air density is 1.2 kgm^{-3}. Making this assumption, and knowing latitude, only information on the pressure gradient is required to permit calculation of the geostrophic wind speed.

3.3 Sources of pressure data considered

Initially, three potential sources of atmospheric pressure data were identified for use in the POWER project:

1. The European Centre for Medium Range Weather Forecasting (ECMWF) – output from an on-going reanalysis of atmospheric data.
2. National Center for Atmospheric Research (NCAR) – 12-hourly data, gridded at a resolution of 5º latitude by 5º longitude. 1899 - present.

3. UK Meteorological Office – daily/monthly mean sea level pressure data for the Northern Hemisphere, gridded from synoptic charts at a resolution of 5º latitude by 10º longitude between 15ºN and 65ºN, and a lower resolution at higher latitudes. 1880 to present.

Of these data sources, the NCAR data set was considered to be the best long-term record of atmospheric pressure available.

However, by the time work on the POWER project commenced (in August 1998), the availability of suitable data had changed. In the intervening period, the National Centers for Environmental Prediction (NCEP) model had been used to reanalyse its source data based on a process of physical interpolation. This has generated readily available, 6-hourly atmospheric pressure data on a 2.5º latitude by 2.5º longitude grid. Moreover, the NCEP data dates back to 1948 and the historical data set is being continuously extended.

Unfortunately ECMWF were unable to supply data in a useable format immediately and consequently this potential source of data was not pursued further. In addition, it was decided that interpolation of the coarse resolution (5º x 10º) UK Met. Office data onto a fine (0.5º) grid would be inappropriate.

As a result, only two sets of atmospheric pressure source data – the NCAR and NCEP data sets - were selected as for detailed consideration as source data. UEA worked with the NCEP data (6 hourly on a 2.5º x 2.5º grid) while CLRC-RAL worked in parallel on the NCAR data set (12 hourly on a 5º x 5º grid). Test geostrophic wind speed vector and stream function plots calculated from the NCEP and NCAR data sets were compared for three sample days in 1990 (for details of the methodology used see sections 3.4 and 3.5). The dates selected represent a severe storm and typical winter and summer days and in each case the plots compared well, both with each other and with some independent validation data.

On this basis it was judged that both the NCEP and NCAR atmospheric pressure data sets would be suitable source data. However, given that the NCEP atmospheric pressure has a finer spatial (2.5º x 2.5º) and temporal (6-hourly) resolution it was considered superior to the NCAR data set. Furthermore, the NCAR data had numerous temporal gaps which made manipulation of the data in FORTRAN programs laborious. In view of this, the NCEP atmospheric data covering a 13 year period (1985 to 1997 inclusive) was selected as the primary source data for the POWER geostrophic wind calculations.

3.4 Interpolation of the pressure data

The NCEP atmospheric pressure data are available on a 2.5º x 2.5º latitude/longitude grid. The geostrophic wind was required on a 0.5º x 0.5º latitude/longitude grid. Therefore, the pressure data had to be interpolated onto the finer grid before performing the geostrophic wind computations. Since pressure is a relatively smoothly varying field at mid-latitudes, interpolation techniques were used that give smoothly varying estimates that are accurate at the original grid nodes. Two methods of interpolation were tested, bi-cubic and bi-cubic spline interpolation.

Since the most testing conditions for interpolation are during severe storms, when pressure gradients are greatest, four storms were used to examine the performance of the interpolation routines against each other and against an independent data set. The independent data used for testing were the surface pressure charts from the European Meteorological Bulletin (EMB). These are contoured by hand from station measurements and provide a rigorous, independent test of the interpolated data.

3.4.1 Bi-cubic interpolation

The main weakness of bi-cubic interpolation is that the user is required to specify derivative information at each grid point (Press et al., 1992). This is usually estimated using numerical methods. The method can give apparently reasonable interpolations that are inaccurate because of the approximate nature of the numerical technique used to specify the derivatives. However, the revised Akima algorithm used in this study provides reliable derivatives.

3.4.2 Bi-cubic spline interpolation

Essentially a variant of bi-cubic interpolation, bi-cubic spline interpolation uses one-dimensional splines to provide the derivative information. The bi-cubic spline provides the smoothest curve possible through the data, in the sense of minimising the mean squared sum of second derivatives (Watson, 1992). A problem with the method is that in regions of high gradient and sharp changes in

direction of the raw data, the interpolation can "overshoot" giving rise to anomalies such as negative rainfall! Mid-latitude gridded pressure data are not normally prone to sharp changes in direction so bi-cubic splines are a particularly useful way of interpolating pressure data. To overcome the problem of overshooting, a spline routine with the facility for introducing "tension" to the spline was used. This gives the technique known as "rubber-sheeting", where the interpolated data fit the original grid accurately and the interpolated points are located on a notional elastic sheet between them that can be pulled to any required level of tautness. To maximise the derivative information in the data, and allow realistic interpolation of low pressure centres between grid nodes, we start with minimal tension and search for evidence of overshooting.

3.4.3 Method of comparison

In a storm situation there are many closely packed isobars thus providing a challenging case study in which to evaluate interpolation techniques. Four storms were chosen, for each the meteorological chart for a time nearest to the time of maximum storm intensity was used. The test domain is 15º W to 15º E, and 45º N to 70º N. Three plots are presented; an isobar plot of the storm at the current time based on the spline-interpolated data, and latitudinal and longitudinal cross-sections of the test (EMB chart) and interpolated data near the centre of the storm. For copyright reasons it is not possible to present a digitized version of the EMB charts. Differences between the test charts and the interpolated data will be described where relevant. However, a general point is worth noting at this stage. The EMB charts have a 5º x 5º latitude/longitude grid. To digitize the cross-sections, we interpolated visually at increments of 2.5 degrees. This means that the cross-sections are not always through the centre of the storm, and that the location of the lowest pressure from the test data may suffer from apparent drift due to the relatively coarse resolution of these data. Finally, although hand contouring introduces a level of skill not available to computer generated contours, it is still prone to error where the data are sparse. Thus, although the EMB charts are expected to be more reliable than any gridded data, and are hence a suitable source of validation data, they may also contain problems in this analysis where pressure gradients are extremely high.

3.4.4 Results of the comparison

Storm of 16 October, 1987

This was the "hurricane" that devastated much of south-eastern England. Figure 3.1 shows the storm before it made landfall, as contoured by GrADS from the 0.5º x 0.5º spline-interpolated pressures. The distribution of pressure about the centre is very asymmetrical, with the region of strong winds being confined to the south-eastern quarter (this makes it something of a textbook storm). This interpolation is a very good representation of the overall pressure pattern observed for this storm. The location of the region of lowest central pressure is virtually identical to that found in the EMB chart. However, even though the 972 mb contour in Figure 3.1 is in roughly the same position as on the EMB chart, the observed gradient within that contour is much greater than indicated by the interpolations in Figure 3.1. This is discussed more fully in the description of the latitudinal and longitudinal cross-sections.

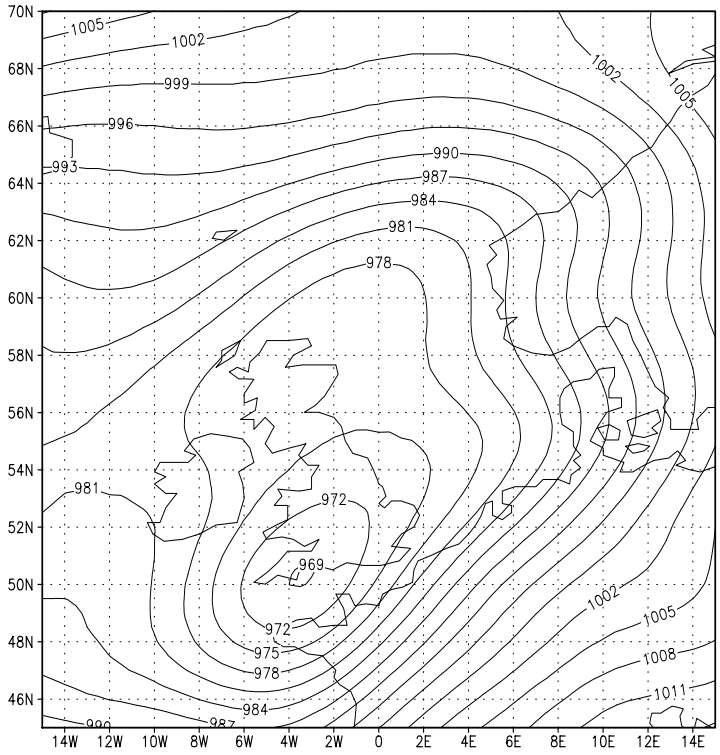

Figure 3.1 00 hrs 16/10/87

Figure 3.2 shows a cross section along 5º W, extracted from the EMB chart at 2.5º intervals (solid line) together with the curves from the interpolated NCEP data (dashed lines). There is very little difference between the results from the two interpolation methods, but both overestimate the minimum pressure by about 15 mb. Other than this the interpolated pressures are in good agreement with the observed data. The reason for the underestimated central pressure is that this storm was a very unusual event with an extremely high pressure gradient over two degrees of latitude/longitude. This is sub-gridscale to our original pressure grid (2.5 x 2.5 degrees). Therefore, the interpolation routines had little information on gradients close to the storm centre. This problem is compounded by the asymmetrical nature of this storm, with virtually all the high wind speeds in the south-eastern quadrant. Fortunately, storms like this are extremely rare. The event is included to demonstrate the errors likely to occur where the original data has insufficient information to perform a reliable interpolation.

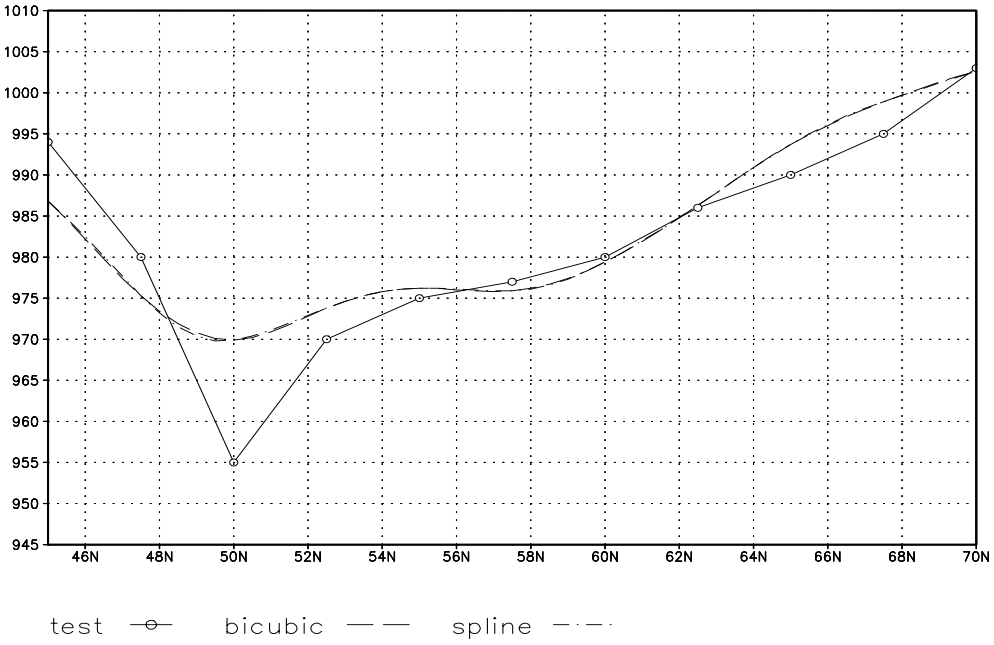

Figure 3.2 00 hrs 16/10/87, cross-section along 5ºW

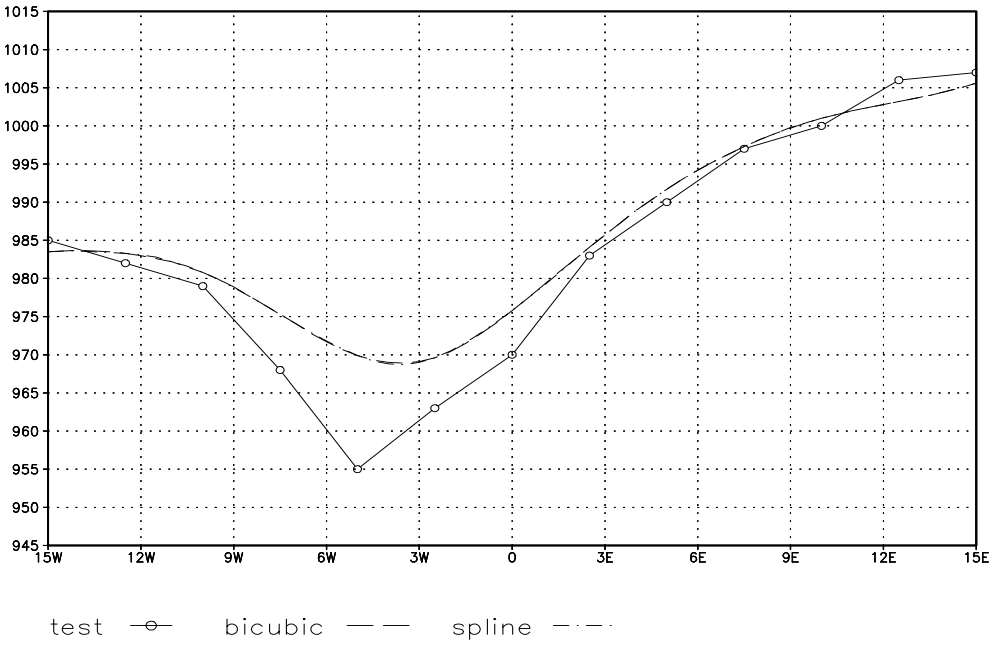

Figure 3.3 00 hrs 16/10/87, cross-section along 50ºN

Figure 3.3 shows a longitudinal cross-section at 50º N of the storm in Figure 3.1. Again, the results from the two interpolation methods are virtually identical and the interpolated data overestimate the central pressure by about 15 mb. The apparent drift in the location of the minimum pressure is an artefact due to sampling the EMB chart at 2.5º intervals.

Storm of 26 January, 1990

This storm caused a severe surge off the Netherlands when centred over Norway for several hours. To give a better cross-section, we show its location 6 hours earlier (Figure 3.4). Again, this is an accurate representation of the EMB chart. The latitudinal cross-section along 2.5º E (Figure 3.5) shows an excellent match between the interpolated and test data, although there is a suggestion that the data sets are not precisely in phase. This is manifested much more strongly in the longitudinal cross-section at 57.5º N (Figure 3.6), and is because the test data are not aligned precisely through the centre of the storm and suffer from the effects of relatively low resolution. Generally, the interpolated data provides an excellent match with the observed, and the central pressure of the storm is within 1 mb of the observed central pressure.

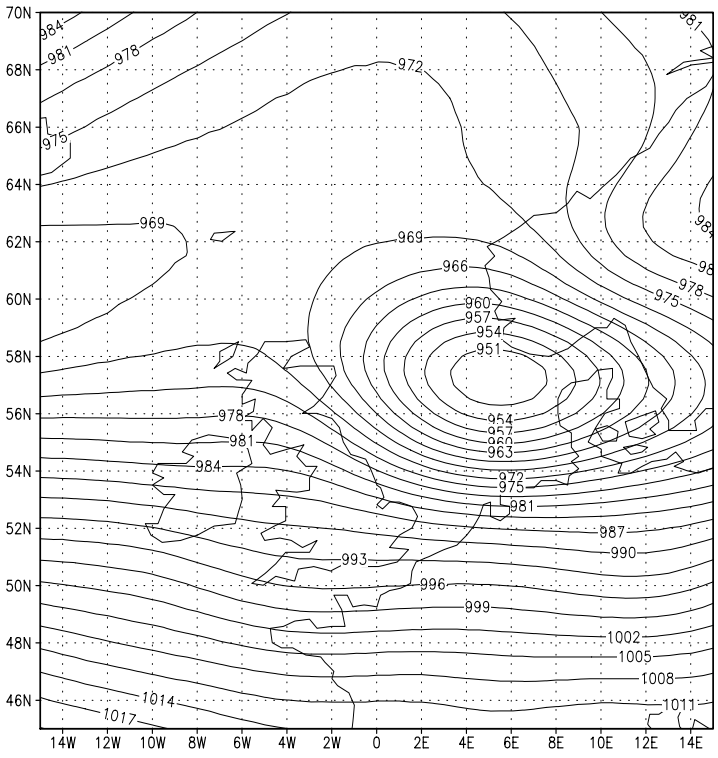

Figure 3.4 00 hrs 26/1/90

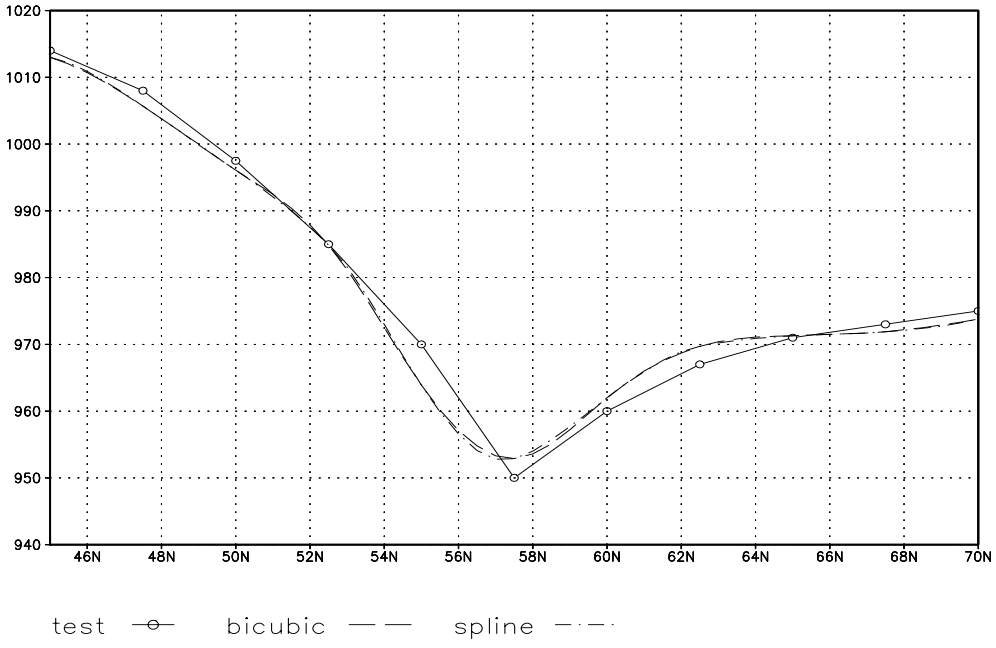

Figure 3.5 00 hrs 26/1/90 cross-section along 2.5ºE

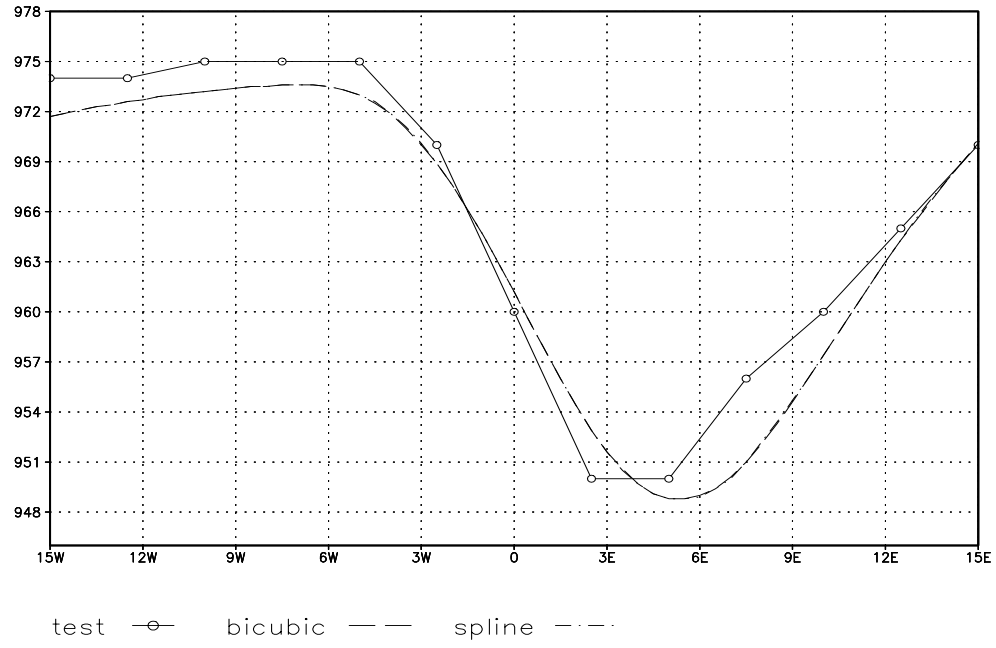

Figure 3.6 00 hrs 26/1/90 cross-section along 57.5º N

Storm of 12 December, 1990

This storm was not particularly severe, but was chosen for test purposes because it had a double storm centre that might not be picked up by the interpolation routine. Unfortunately, the centre associated with the parent low is beyond the northern limits of the test map, but it can be inferred from the way the isobars open in the top right corner of the map, indicating a centre at about 72º N and 16º E. This is an accurate representation of the observed chart, with the location of the centre shown in Figure 3.7

closely matching the observed location and the alignment of the axis between the two centres, along the coast of Norway, matching the observed axis perfectly.

Although the test data in the cross sections (Figures 3.8 and 3.9) suffer from apparent drift, there is a good match between the observed and interpolated data. The interpolated minimum pressure is within 3 mb of the observed minimum.

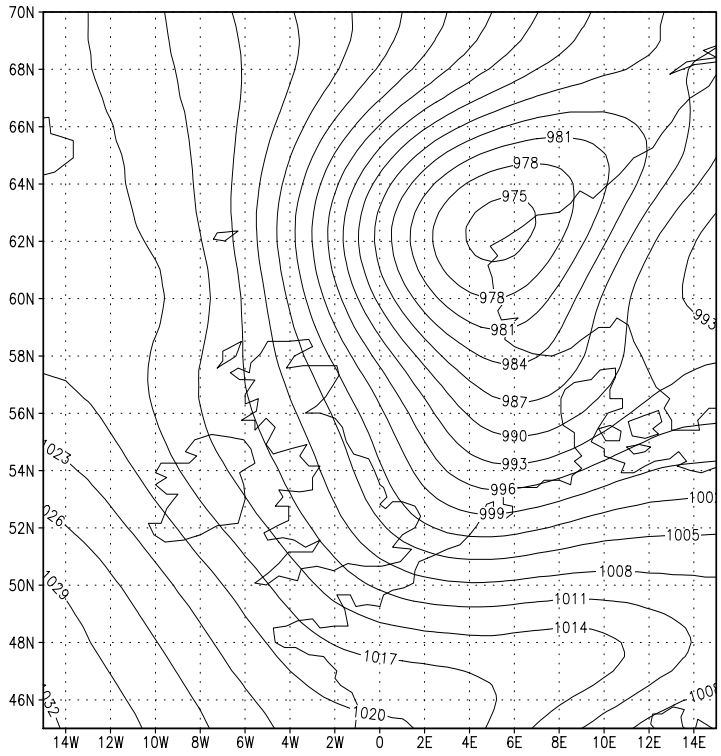

Figure 3.7 00 hrs 12/12/90

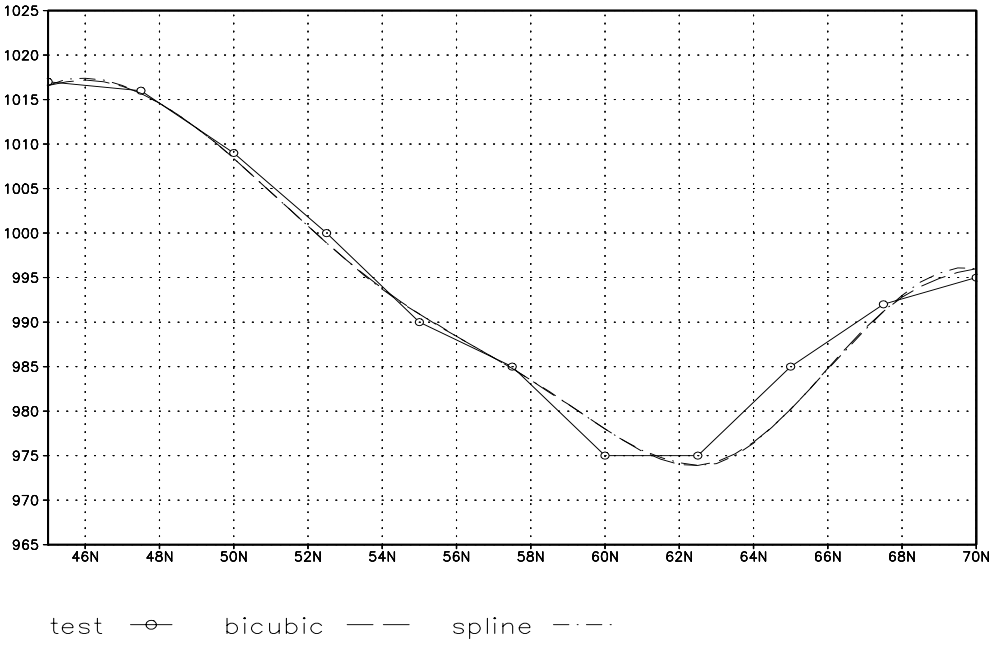

Figure 3.8 00 hrs 12/12/90 cross-section along 5º E

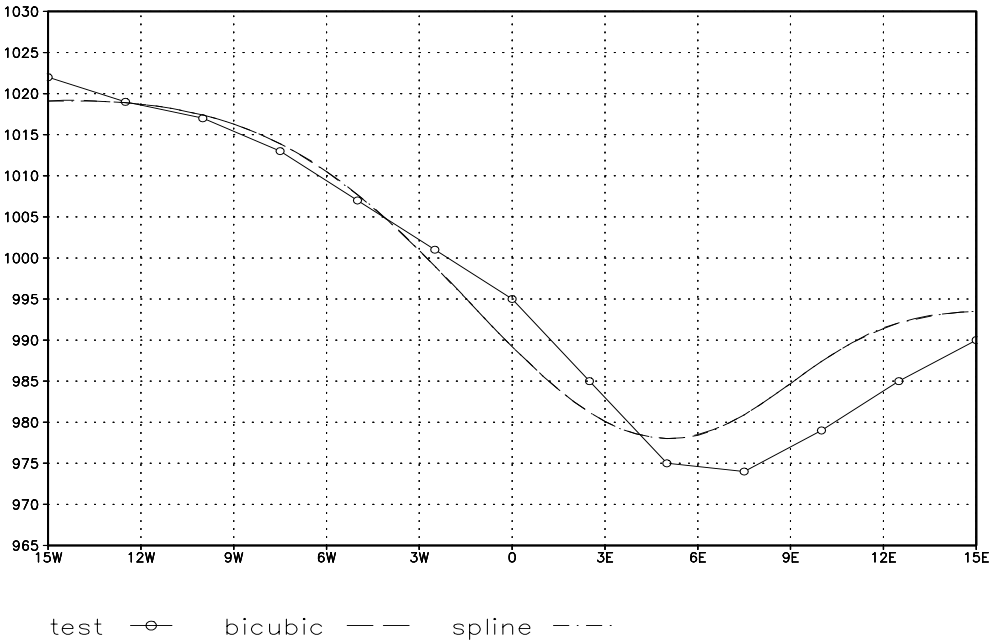

Figure 3.9 00 hrs 12/12/90 cross-section along 60º N

Storm of 5 January, 1991

This storm caused severe surges in the Irish Sea. There is good agreement between the observed pressure field and the interpolated field shown in Figure 3.10. The cross-sections (Figures 3.11 and 3.12) indicate that, although the interpolations give a good representation of the pressure field, they underestimate the central pressure of the depression by about 6 mb (Figure 3.12).

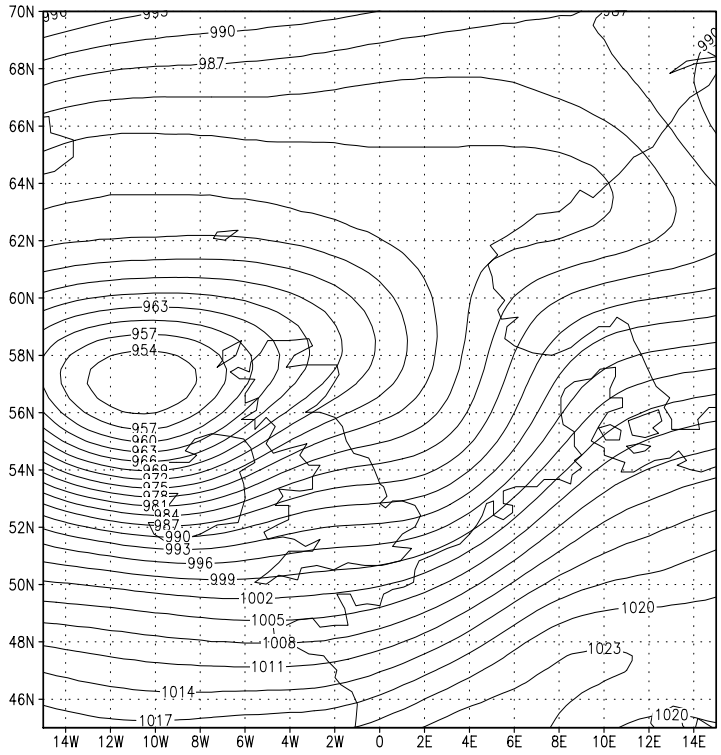

Figure 3.10 12 hrs 5/1/91

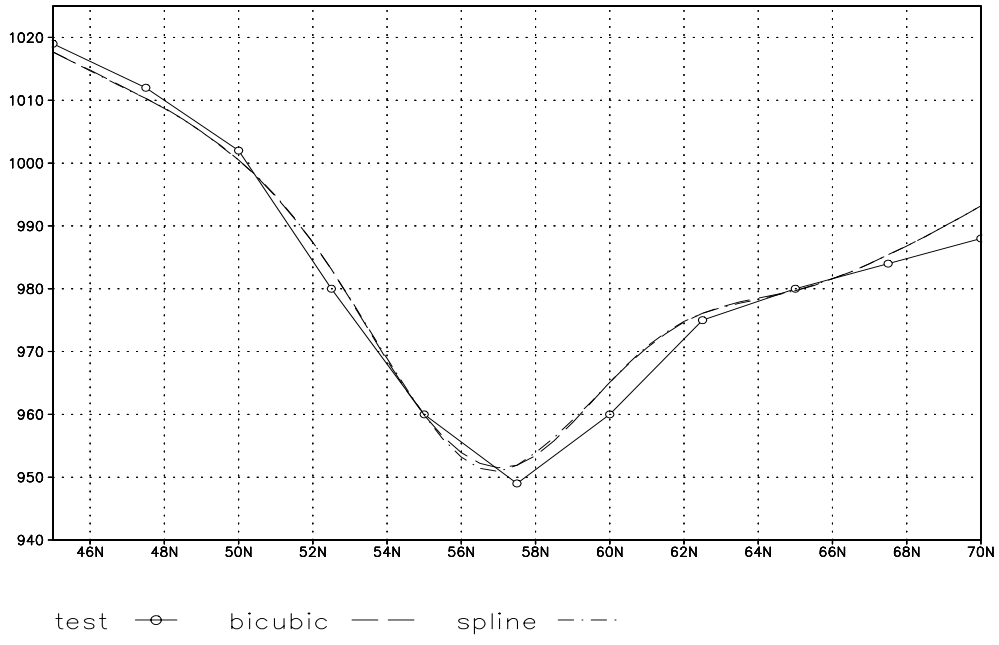

Figure 3.11 12 hrs 5/1/91 cross-section along 10º W

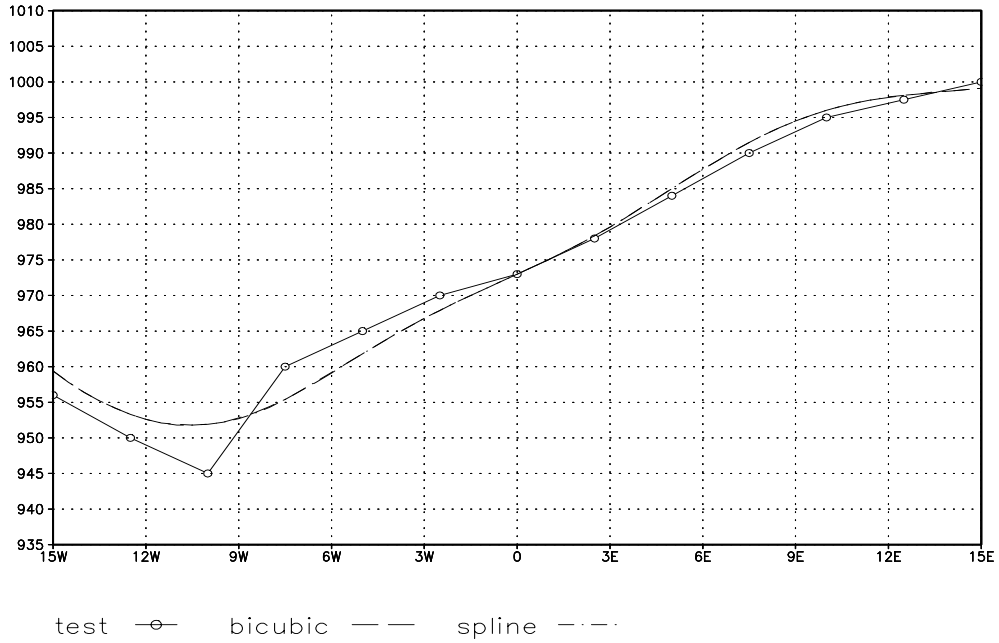

Figure 3.12 12 hrs 5/1/91 cross-section along 57.5º N

3.4.5 Conclusions regarding choice of interpolation scheme

The interpolation methods used in this study are in very close agreement in all the severe storm case studies, indicating that either method would be suitable for interpolating the NCEP pressure data onto a 0.5º x 0.5º latitude/longitude grid. The test data indicates that the interpolated data gives an accurate representation of mid-latitude storms. The only exception to this is for storms with gradients that are sub-gridscale to the original gridded pressure data. However, one should consider that the test data themselves are also the product of some interpolation. Although we consider them a good representation of the pressure field, they are only exact when the contour coincides with a meteorological station. There are some instances where it is impossible to say which data set is in error when the match is less than perfect. For example, the occasions when the test and interpolated datasets seem out of phase near the storm centre are due to the relatively coarse resolution of the digitised EMB test data.

We decided to use the bi-cubic spline method of interpolation for the remainder of this study since, with pressure data, it gives essentially the same results as Akima's bi-cubic interpolation and is faster to compute. There is no indication that the spline interpolation overshoots in conditions of very severe gradient.

3.5 Calculating the geostrophic wind

The 6-hourly interpolated atmospheric pressure data for the period 1985-97 was used to calculate the sea level pressure gradients in the westerly and southerly directions at each point in the 0.5º by 0.5º latitude/longitude grid. These components of pressure gradient were then converted to components of geostrophic wind using equations 3.5 and 3.6:

$$U_g = -\frac{1}{f_c \rho}\frac{\partial p}{\partial y} \qquad 3.5$$

$$V_g = -\frac{1}{f_c \rho}\frac{\partial p}{\partial x} \qquad 3.6$$

where:

U_g and V_g are the westerly and southerly components of the geostrophic wind speed respectively
f_c is the local Coriolis force for the given latitude
ρ is the density of air
$\partial p/\partial y$ is the component of atmospheric pressure gradient from west to east
$\partial p/\partial x$ is the component of atmospheric pressure gradient from south to north

3.6 Testing the geostrophic wind calculated from interpolated pressure data

3.6.1 Introduction

Here, we test the success of the procedure for calculating the geostrophic winds (see sections 3.4 and 3.5) by comparing the results with the surface wind field calculated by NCEP and output as part of the reanalysis data on a 2.5º x 2.5º latitude/longitude grid. Although the wind fields should not be identical, since the NCEP winds will have slightly different directions and speeds because of the effects of surface friction, there should be sufficient similarity to identify any errors (particularly systematic errors) in the computation of the geostrophic wind.

For testing. we selected three dates from a sample year, to include a severe storm, a winter day and a summer day with relatively light winds. The test data are presented in three formats for each of the three dates: maps of resultant wind vectors, maps of stream function (directional contours of the flow of air), and a table of comparative summary statistics.

3.6.2 The nature of the “Geostrophic Wind"

A more detailed explanation of the geostrophic wind can be found in standard meteorological texts, for example, James (1994). Here we concentrate on testing the data produced for POWER by comparing these to the surface wind calculated by NCEP. The geostrophic wind is a theoretical wind calculated from surface pressure data. A balance is assumed between the flow of air from high to low pressure regions and the effects of the rotation of the Earth as manifested in the “Coriolis Effect”. The geostrophic wind flows parallel to the isobars (contours of equal surface pressure), and reflects the flow of air in frictionless conditions. This can be taken to be above 500-1000 m, but varies greatly depending on factors such as the nature of the underlying surface, in terms of topography and roughness, and on the stability of the overlying air. Because of surface friction, the wind at 10 m will be different from the geostrophic wind in speed and direction. The relationship is complex, depending on the square of the wind speed, the surface roughness, the effects of funnelling due to surface topography, and the stability of the atmosphere.

In very simplistic terms, we can describe the main effects of friction to be:

- Slowing due to frictional retardation caused by the roughness of the surface. One would expect wind speeds at 10 m to be roughly 30% of the geostrophic wind speeds over land and roughly 60% of geostrophic wind speeds over the sea. The different amount of slowing is due entirely to the difference in surface roughness between the land and the sea. The slowing increases with wind speed.

- Turning of the wind to the left around low pressure centres in the Northern Hemisphere. The amount of turning is a function of height and normally approximates the simple spiral defined by Ekman. The change in direction of the 10 m wind relative to the geostrophic wind could be of the order of 15 to 20 degrees.

In this study, we are calculating the geostrophic wind from pressure data at 0.5º x 0.5º latitude/longitude nodes. The calculations are performed using pressure gradients over a particular pressure node from 1º north and south of the node (that is, gradients over 2º of latitude), and 2º east and west of the node (gradients over 4º of longitude). The doubling of the distance for longitude gradients roughly counters the effect of convergence of longitude lines as one approaches the Pole. This gives an approximately square box for the pressure gradient calculations of about 230 km (varying with latitude).

Storm of 26 January, 1990

Before discussing the particular features of this test it is important to note adjustments to the data that are made for pragmatic reasons. To display the wind vectors of the calculated geostrophic wind at their true resolution (0.5º x 0.5º) would result in a meaningless forest of lines. Therefore, we skipped all vectors other than those at 2.5º x 2.5º intervals, giving vectors at the same points for the test and geostrophic data. Since the stream function plots are contours, all available data can be used. This means that the stream function of the geostrophic data can display small circulations that are missing from the test plots since they are sub-grid scale to those data. This occurs over Spain, for example, when comparing Figures 3.19 and 3.20.

The wind vectors shown in Figures 3.13 and 3.14 indicate that the calculated geostrophic wind (Figure 3.14) compares superficially well with the surface wind field from NCEP (Figure 3.13). However, the scaling (indicated beneath each vector plot) shows that a vector for geostrophic wind speeds represents twice the wind speed of a vector the same size on the surface wind speed map. This is partly because of the effects of surface friction reducing the wind speeds at the surface and partly because of differences in the spatial resolution of the raw data. The geostrophic winds are computed from pressure data that is at a spatial resolution 5 times higher than that of the surface winds. Around the storm centre, where pressure gradients and wind speeds are highest, the better spatial resolution allows the computation of geostrophic wind speeds that are sub-grid scale to the surface wind data. Effectively, in this crucial region, the test data are smoothed in space and cannot reflect the rapid changes in wind speed over a small area that are encountered around a very severe storm.

The plots of streamfunction (Figures 3.15 and 3.16) appear to be different in the region of the storm centre (off western Denmark). In fact, both stream function plots are correct. In figure 3.16, the wind is frictionless and runs parallel to the isobars, so the stream function plot is essentially the same as a contour plot of surface pressure. In Figure 3.15, we see the effects of surface friction turning the direction of the wind towards the centre of the storm (to the left in the Northern Hemisphere), so that the concentric contours around the storm centre have more of the appearance of a vortex.

The statistics in Table 3.1 are calculated across all grid points and indicate that the standard deviation and range of the u and v components of the geostrophic wind field are much higher than those of the test data. This is to be expected given the differences in scaling already noted in the discussion of Figures 3.13 and 3.14.

Table 3.1 Wind speed statistics from the test and interpolated data for 00 hrs 26/01/90

Wind component	**Minimum**	**Maximum**	**Standard deviation (n-1)**
Test u (m/s)	-19.2	33.9	8.91
Interpolated u (m/s)	-36.1	62.0	14.42
Test v (m/s)	-18.6	21.1	5.73
Interpolated v (m/s)	-39.4	31.2	10.21

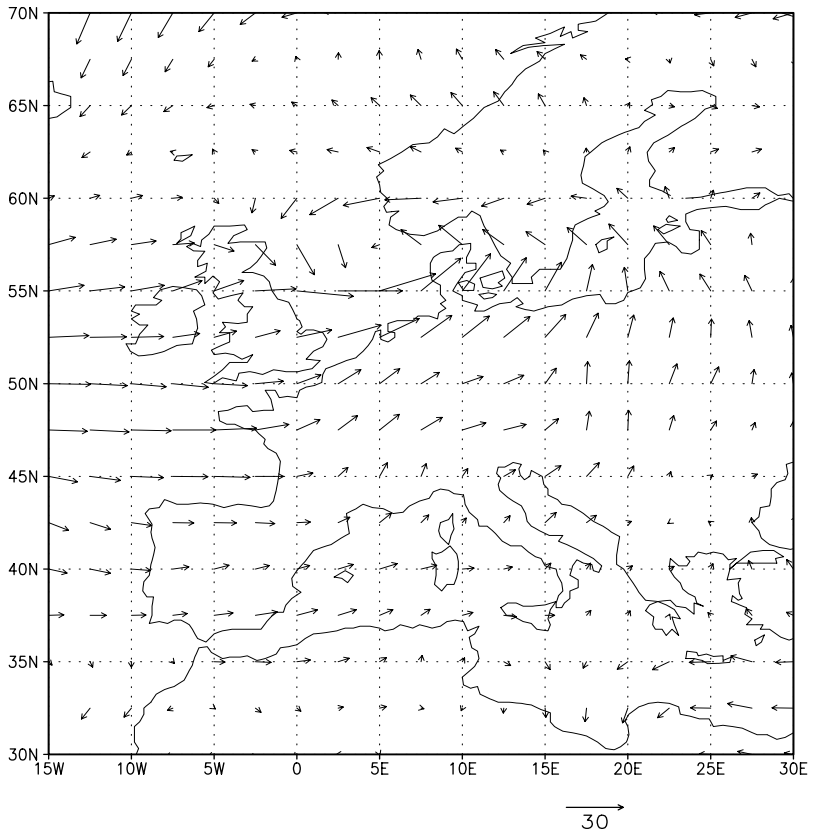

Figure 3.13 Wind vectors from test data for 00 hrs, 26/01/1990

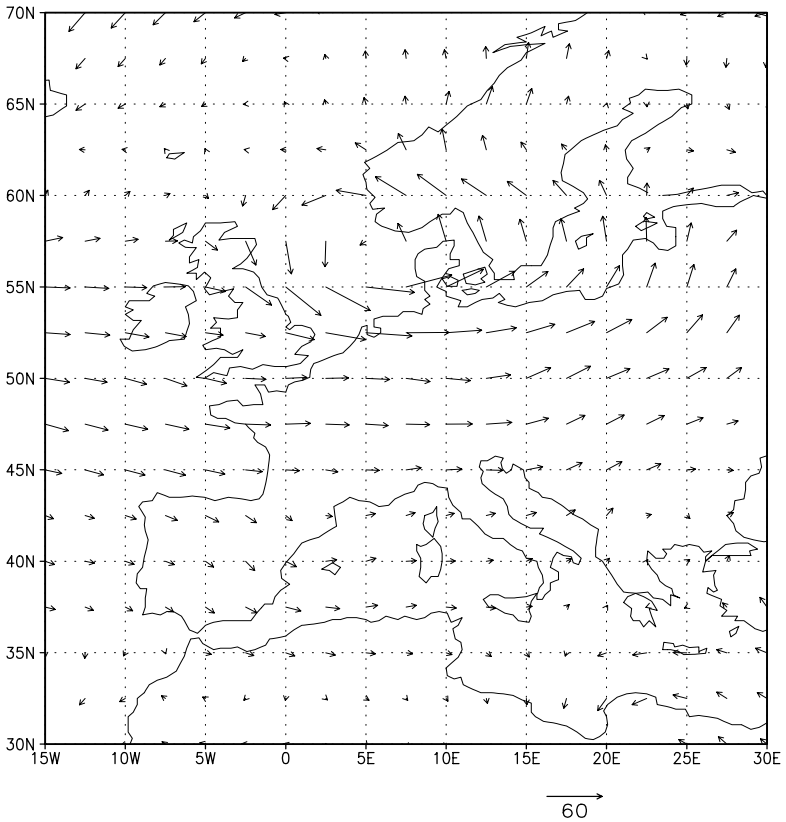

Figure 3.14 Wind vectors from interpolated pressure data for 00 hrs, 26/01/1990

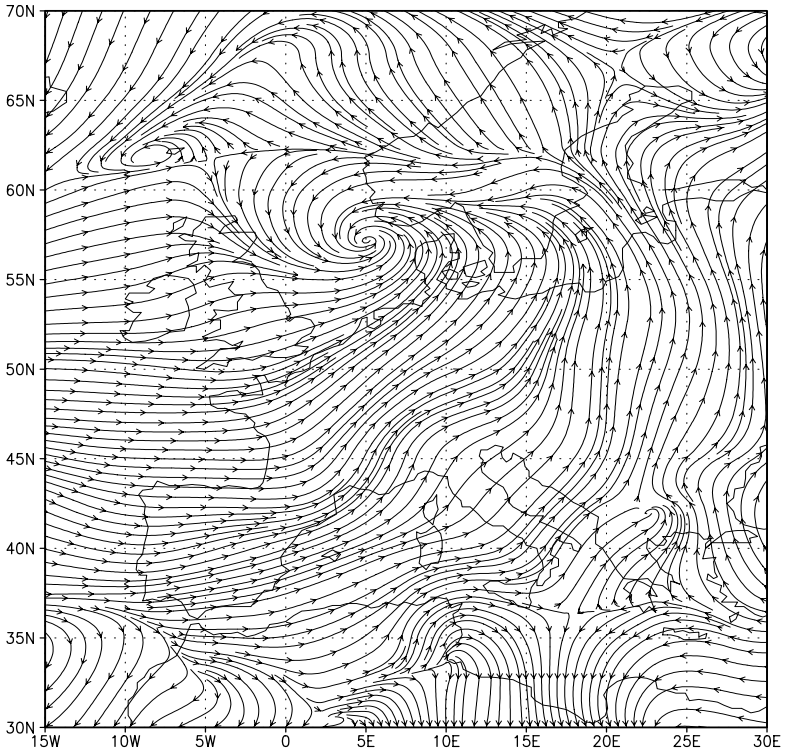

Figure 3.15 Stream function from test data for 00 hrs, 26/01/1990

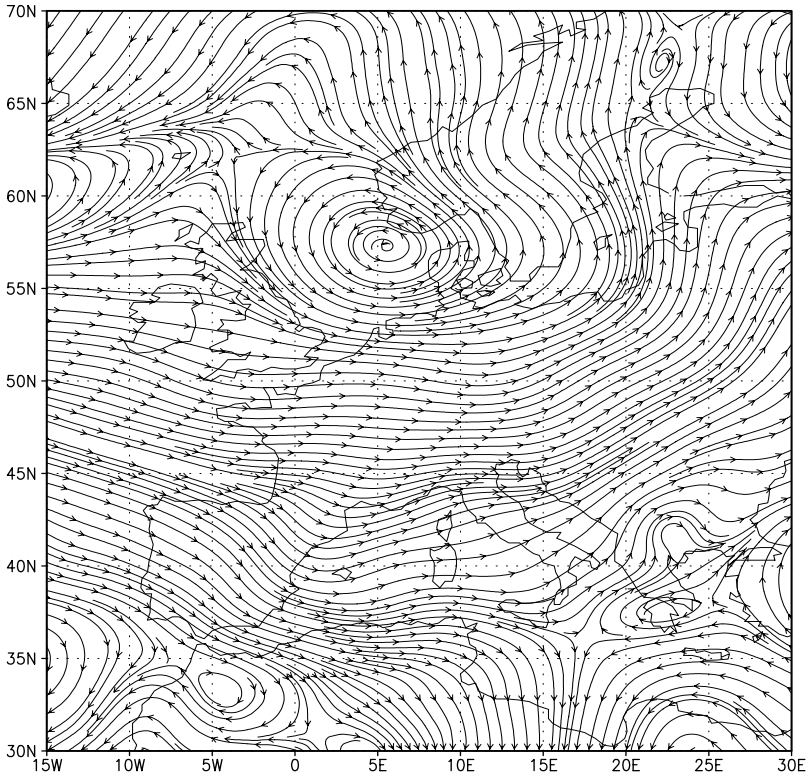

Figure 3.16 Stream function from interpolated pressure data for 00 hrs, 26/01/1990

Winter day, 1 January, 1990

The wind speeds for a "normal" winter day compare much better than in the extreme case of the severe storm used in the previous example. Figures 3.17 and 3.18 show good agreement between the patterns and scaling of wind vectors. The plots of stream function for the test and interpolated data (Figures 3.19 and 3.20, respectively) indicate comparable fields with the effect of cross-isobar flow evident at every pressure centre shown in the test data chart (Figure 3.19).

Although the statistics of the u components of the wind compare well between the test and interpolated fields (Table 3.2), there is a large discrepancy between the v components. Since the geostrophic wind has to have higher *resultant* wind speeds than the surface wind, the way this is reflected in the u and v components varies with the configuration of surface pressure at a particular time. Thus, there is no significance in the fact that on this occasion the v component shows the discrepancy.

Table 3.2 Wind speed statistics from the test and interpolated data for 00 hrs 01/01/90

Wind component	**Minimum**	**Maximum**	**Standard deviation (n-1)**
Test u (m/s)	-16.8	16.2	5.46
Interpolated u (m/s)	-17.6	17.4	6.45
Test v (m/s)	-8.2	13.5	4.68
Interpolated v (m/s)	-17.5	22.6	7.93

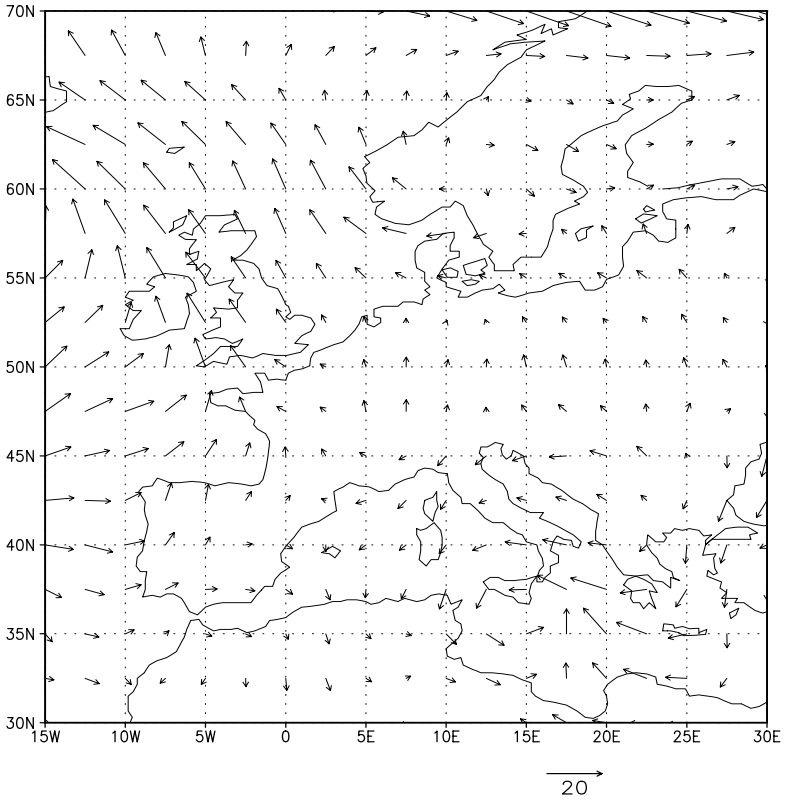

Figure 3.17 Wind vectors from test data for 00 hrs, 01/01/1990

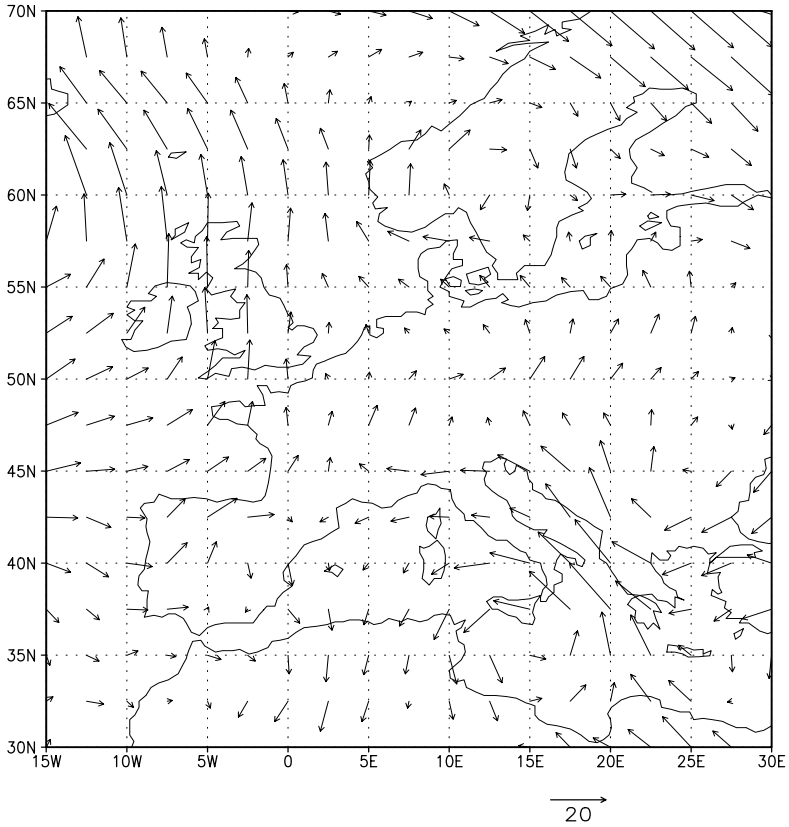

Figure 3.18 Wind vectors from interpolated pressure data for 00 hrs, 01/01/1990

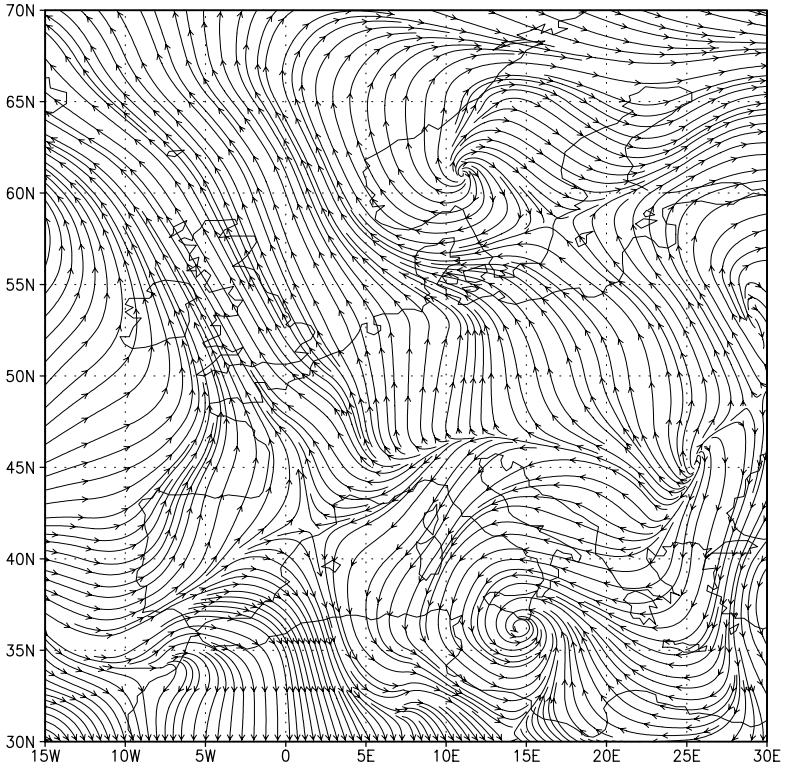

Figure 3.19 Stream function from test data for 00 hrs, 01/01/1990

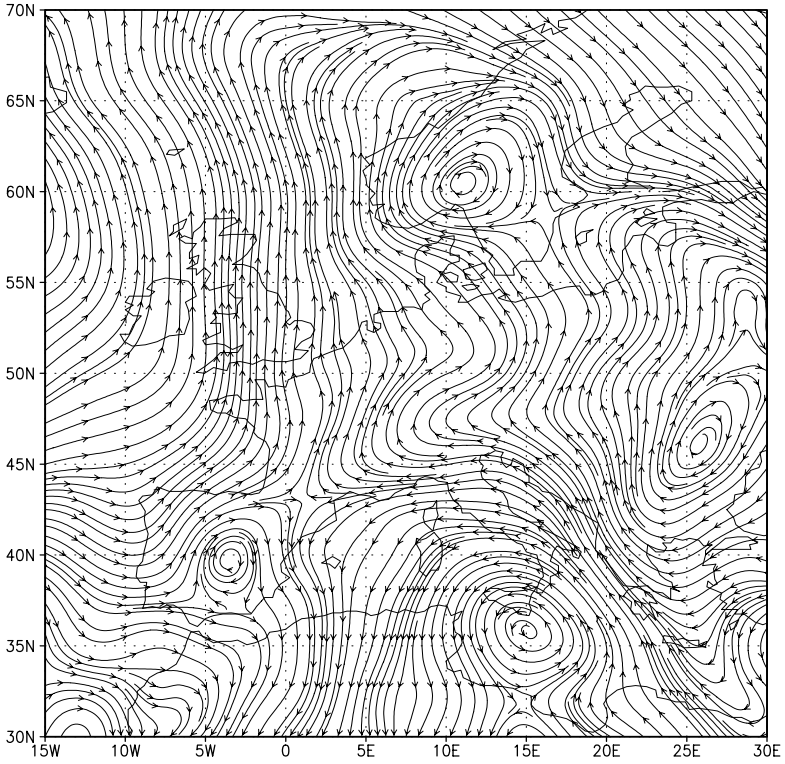

Figure 3.20 Stream function from interpolated pressure data for 00 hrs, 01/01/1990

Summer day, 24 June, 1990

In many ways, the example of a summer day is the most severe test of the geostrophic winds since the hemispheric circulation is at its weakest.

Figures 3.21 to 3.24 indicate that the geostrophic wind calculated from the interpolated pressure data is correct. The scaling for the geostrophic and test wind vectors (Figures 3.21 and 3.22) is different, but this simply reflects the higher speeds of the frictionless flow. The statistics in Table 3.3 show that the interpolated u and v components of the geostrophic wind have higher variability than the test u and v components.

Table 3.3 Wind speed statistics from the test and interpolated data for 00 hrs 24/06/90

Wind component	Minimum	Maximum	Standard deviation (n-1)
Test u (m/s)	-10.8	13.9	4.10
Interpolated u (m/s)	-18.0	22.0	6.18
Test v (m/s)	-12.8	12.6	4.61
Interpolated v (m/s)	-14.5	18.4	5.79

3.6.3 Conclusions regarding comparison of POWER geostrophic winds with NCEP surface winds

The examples shown in this section indicate that the geostrophic wind calculated for POWER has consistent variability with the surface wind and is, therefore, a good basis for the development of the models to predict near-surface winds in the far offshore and near-shore zone.

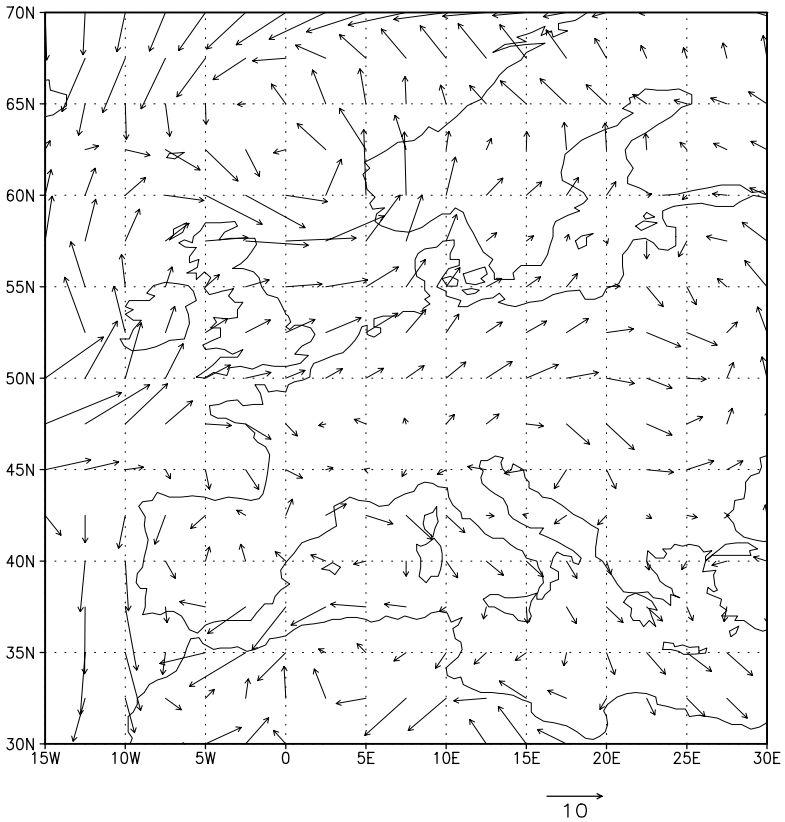

Figure 3.21 Wind vectors from test data for 00 hrs, 24/06/1990

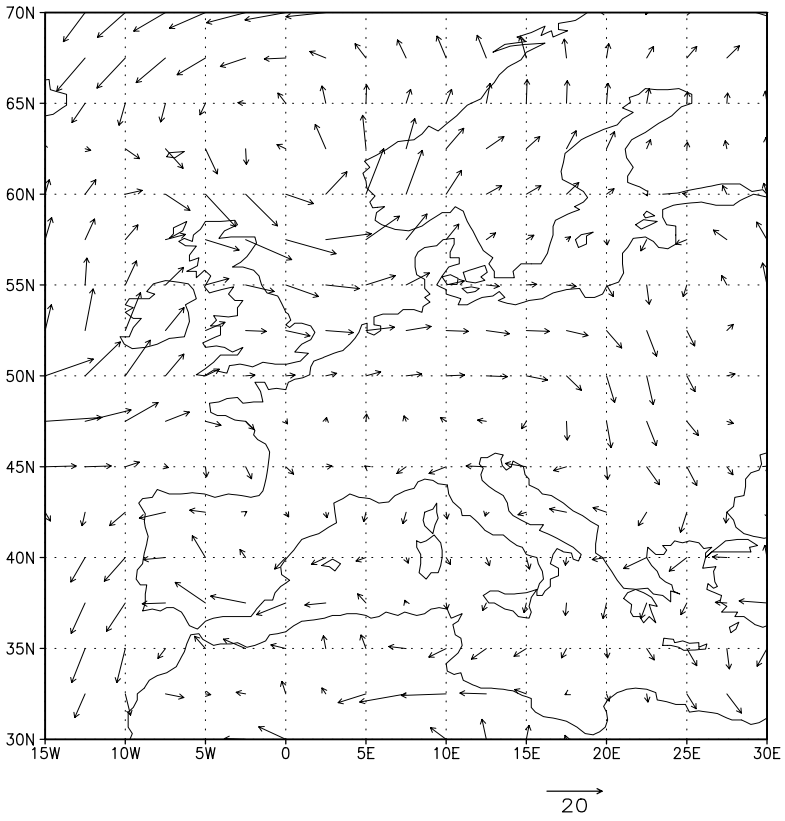

Figure 3.22 Wind vectors from interpolated pressure data for 00 hrs, 24/06/1990

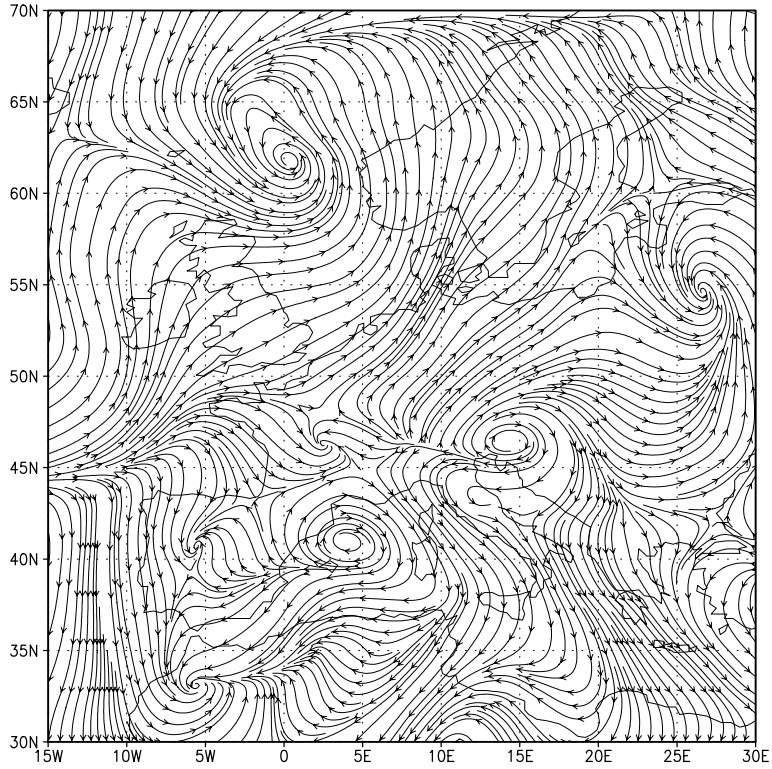

Figure 3.23 Stream function from test data for 00 hrs, 24/06/1990

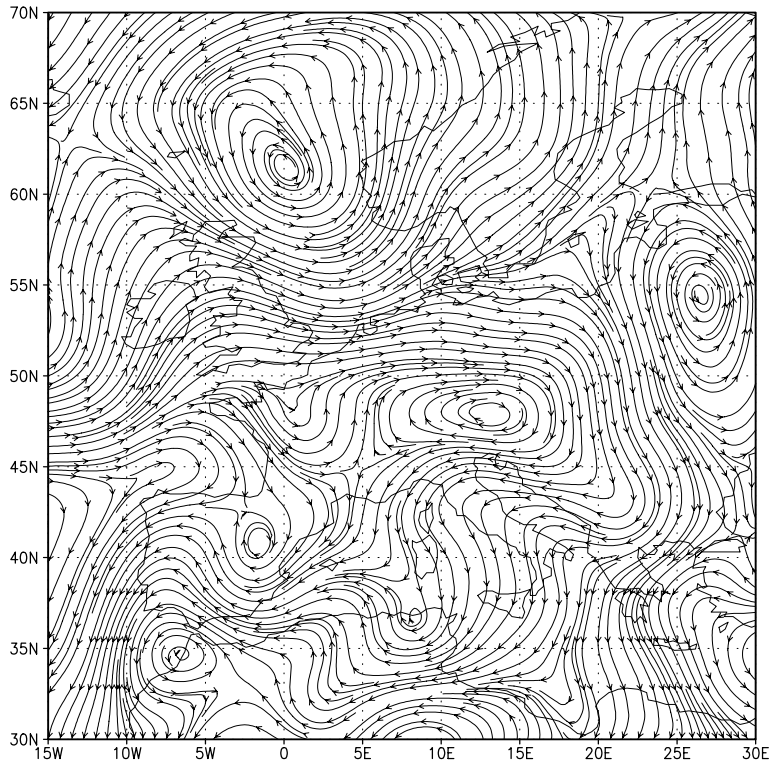

Figure 3.24 Stream function from interpolated pressure data for 00 hrs, 24/06/1990

3.7 Using radiosonde data to validate the geostrophic wind

3.7.1 Introduction

In Section 3.6, we tested the geostrophic winds computed from pressure data interpolated onto a 0.5º x 0.5º latitude/ longitude grid by comparing with the surface wind field calculated by NCEP (Kalnay et al., 1996) on a 2.5º x 2.5º latitude/longitude grid. Although this approach would identify any errors in the calculation, it can only be used as a very general test of the validity of the calculated wind field, since the geostrophic wind is a frictionless wind, representing flow 500 to 1000 m above the surface. Furthermore, the surface wind field used for testing is only partly based on observations, much of it is derived from theoretical computations performed using a numerical model. Here we use observations from radiosonde ascents to compare the observed frictionless flow with the theoretical wind derived from the assumptions of geostrophic theory.

For our initial analysis, we take the three dates from 1990 used in Section 3.6. These include a severe storm, a winter day and a summer day with relatively light winds. For each date we present charts of the geostrophic wind speed and direction, superimposed with the appropriate radiosonde observations, for three successive 12-hourly time steps. Similar plots are then presented for a date in 1997, to ensure that the initial findings are consistent and to provide a preliminary assessment of changes in the radiosonde network.

Although the charts provide a detailed overview of the relationship between the geostrophic wind and the observed frictionless wind, it is only possible to consider a small number of timesteps in this way. To examine long term relationships, we provide comparative summary statistics of the geostrophic wind speeds and radiosonde observations for the whole of 1990 and 1997. We conclude that the geostrophic wind is an excellent representation of frictionless flow over the POWER study area.

3.7.2 The Radiosonde Data

Radiosonde data were obtained from the British Atmospheric Data Centre (BADC) for the period 1990 to mid-1998 from an extensive network of European stations. The observation interval ranges from 3 to 12 hours and measurements are often recorded at different heights at different stations. This does not matter for our purposes, since we can use test observations from a wide band of heights to represent frictionless flow. There can be large numbers of missing values, particularly during storm conditions.

As we are primarily interested in the near-shore and far offshore wind fields, and it is desirable to use radiosonde data free from the effects of local topography, we selected coastal radiosonde stations lying below 100 m above msl. This subset of stations was further reduced by a requirement that they have a recording programme covering the period 1990 to mid-1998 and observations at 00 hrs and 12 hrs for each day. Although this report does not use data over the whole of this period, a continuous programme of measurements indicates that the stations are permanent and available for more extensive study if needed. The locations of the 37 radiosonde stations fulfilling these conditions are shown in Figure 3.25. The numbers and division into sub-basins are supplied for reference in later sections.

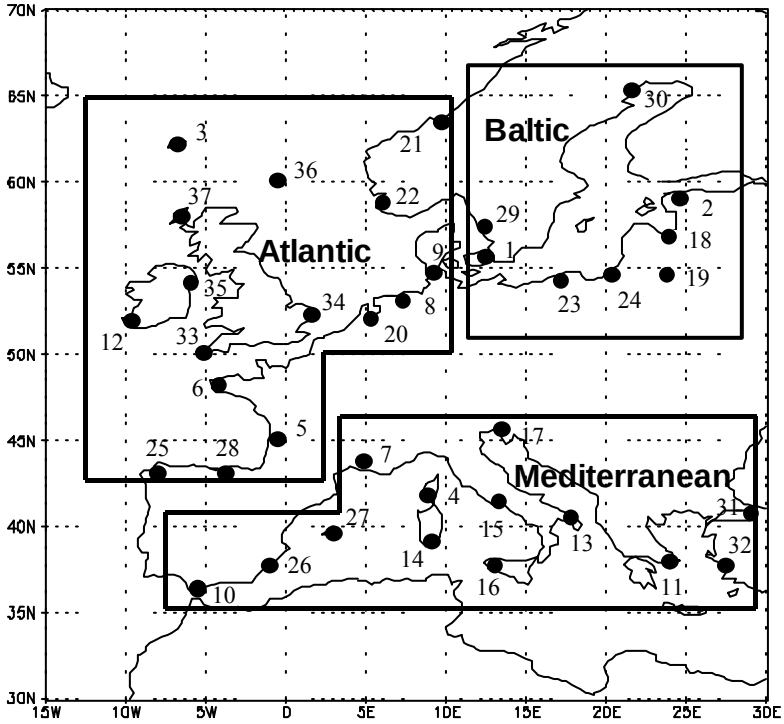

Figure 3.25 Locations of the radiosonde stations used in this report

To accommodate the need to select radiosonde wind speeds and direction from above the friction layer, we extracted these variables for the first occurrence of data at a height between 600 and 900 m. This range of heights was selected empirically as covering a large enough range to minimise missing values and retaining the characteristics of frictionless flow. It is important to note that the "correct" height for measuring frictionless flow varies a great deal depending on factors such as local atmospheric stability, surface topography, and circulations aloft. The latter point partly explains why we need an upper limit to our range even though all winds above a certain level will be frictionless. There are different regimes of horizontal flow at various levels in the atmosphere. Therefore, we need to try to ensure that our frictionless flow is representative of flow at the surface with friction removed, and not influenced by flow at a greater height. The problem is illustrated using the radiosonde observations shown in Table 3.4.

For one example time step, Table 3.4 illustrates the increase in wind speeds and change in direction with height. Between the surface and 813 m, these changes are in accordance with Ekman theory. Between 813 m and 980 m the linkage with the effects of surface friction is ended as wind speeds start to decline with height and the wind direction starts to change in the opposite direction. It is interesting to note that the difference in wind direction between 40 m and 813 m is 30 degrees. McIlveen (1992) states that the maximum value of the change in wind direction between the surface and the gradient (frictionless) layer "seldom exceeds 30 degrees". Therefore, the optimum frictionless wind speed and direction from the data in Table 3.4 are at 813 m. This is also the only value on this time step that falls within our search range of 600 to 900 m height. It should be noted that these data were chosen to illustrate the point. Generally, the patterns are not so clear cut, although the appropriate height for frictionless flow is usually evident.

We now compare the geostrophic wind with the radiosonde observations for each of our sample dates. Although a detailed examination of the wind field on particular time steps is likely to reveal occasional incorrect readings from the radiosondes, we will ignore these and concentrate on the overall match with the geostrophic wind. Where radiosonde information appears to be consistently incorrect, however, we will point this out.

Table 3.4 Sample radiosonde data

Pressure (mb)	Height (m)	Wind direction	Wind speed (knots)
746	2580	115	12
800	2010	130	15
850	1510	135	18
899	1050	145	19
906	980	145	20
925	813	150	20
977	360	145	17
1000	172	140	11
1016	40	120	6

Storm of 26 January, 1990

A few general comments about the way the data in the validation exercises are presented are appropriate here. Although contour maps are not the method normally used to display wind speeds, they are chosen here since they facilitate comparison with the station observations. Radiosonde wind speeds are plotted in a large bold font to distinguish them from the contour labels for the geostrophic data. Although there are potentially 37 radiosonde sites to include in the plots, in all the examples there are several sites with no readings at any given time. Missing values were omitted from the plots, so the locations of radiosonde data can apparently differ between plots depending on the availability of data.

With wind direction, contouring is not practicable because of the discontinuity at 360/0 degrees. Therefore, we present wind direction by plotting the value at each radiosonde site. The adjacent value in brackets is the geostrophic wind direction at the nearest 0.5 degree grid point. So, for example, in Figure 3.27, the frictionless wind direction from the radiosonde in the region of London is 210 degrees, and the corresponding geostrophic wind direction is 234 degrees.

Figures 3.26 to 3.31 show the comparative wind speed and direction for 12 hours preceding the storm, the time of the storm, and 12 hours after the storm. Three time steps are included to compensate for missing values in the radiosonde data. There tend to be more missing values when wind speeds are high.

12 hrs, 25/1/1990

Figure 3.26 shows that for this timestep, in the region of highest geostrophic wind speeds (50-55 m/s over the south of England), wind speeds are underestimated at the nearest radiosonde station by about 20 m/s. This is not surprising when one considers that this was one of the most severe storms to strike the UK and that virtually all radiosondes in the region display missing values for this time step. At most other locations, where the wind speeds are lower, there is good agreement between the wind speeds from the radiosonde data and the geostrophic wind speeds.

There is generally good agreement between the observed and calculated wind direction shown in Figure 3.27.

00 hrs, 26/1/1990

Twelve hours later, the storm centre has shifted over the North Sea (Figures 3.28 and 3.29). There are still large numbers of missing values in the region of the storm centre and the radiosonde wind speeds near the centre (Figure 3.28) appear to be underestimated by about 20 m/s). Away from the storm centre, however, there is generally good agreement between the geostrophic wind speeds and those from the radiosonde ascents.

Again, there is generally good agreement between the observed and calculated wind direction shown in Figure 3.29.

12 hrs, 26/1/1990

As the storm weakens and moves over Scandinavia, there is a marked reduction in the number of missing values (over the UK, for example, see Figures 3.30 and 3.31), which is a clear indication that high wind speed conditions have a damaging influence on the collection of radiosonde data. A preliminary assessment suggests that the cutoff for reliable radiosonde wind speeds is in the region of 30 m/s.

The pattern of agreement between geostrophic wind speed and direction and the corresponding radiosonde data is the same as for the previous time steps. In the region of the storm centre, radiosonde wind speeds appear to be underestimated by about 10 m/s.

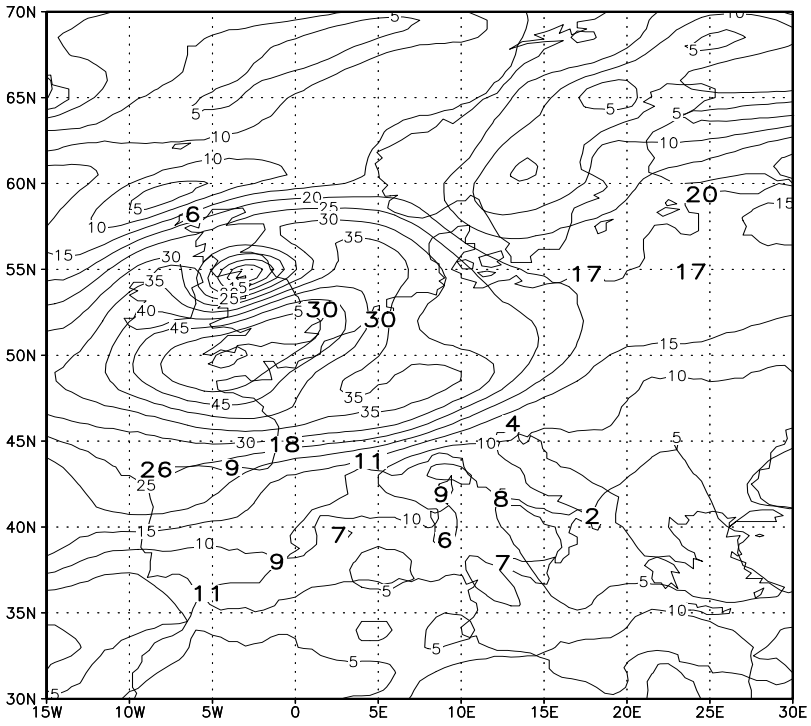

Figure 3.26 Wind speed (m/s) for 12 hrs, 25/01/90

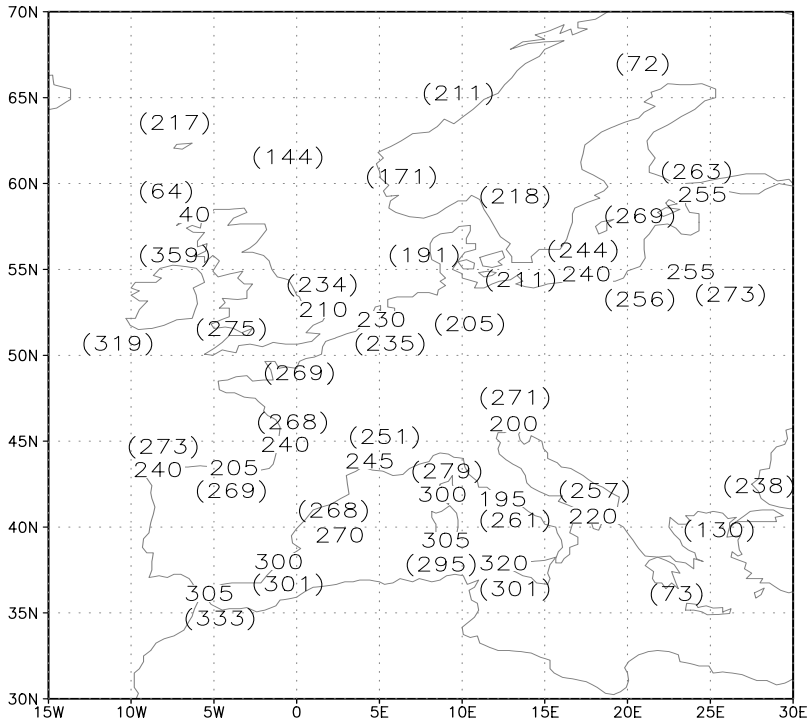

Figure 3.27 Wind direction for 12 hrs, 25/01/90

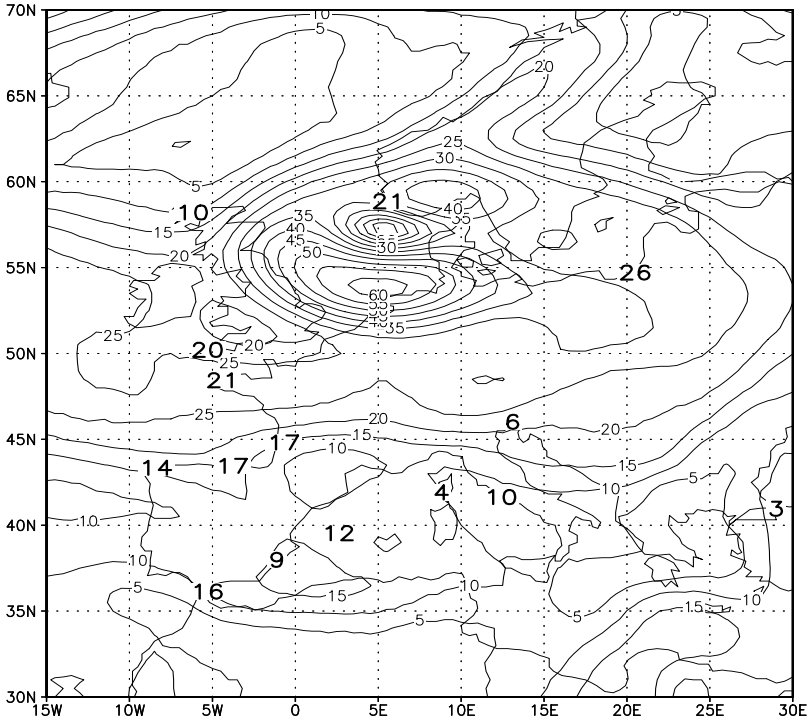

Figure 3.28 Wind speed (m/s) for 00 hrs, 26/01/90

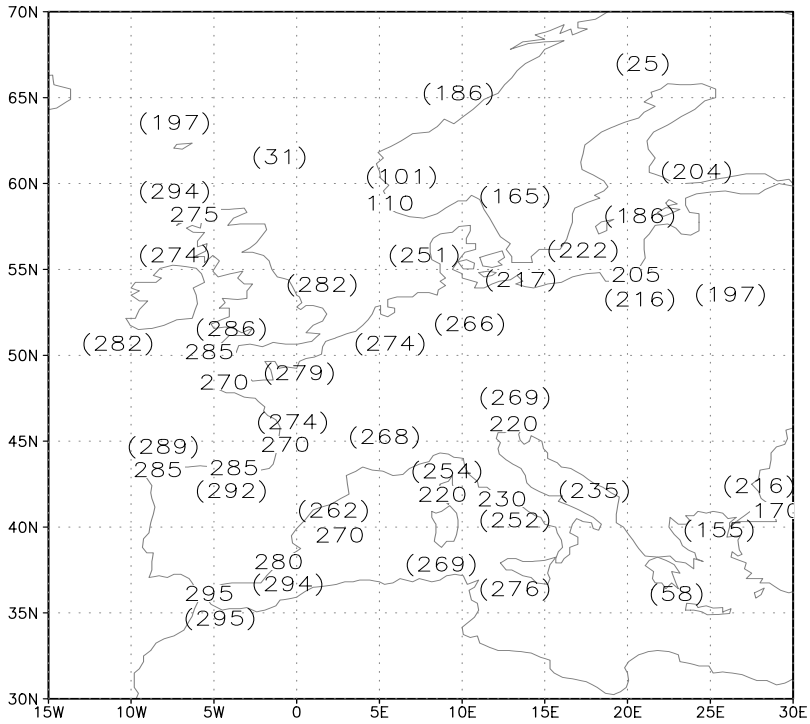

Figure 3.29 Wind direction for 00 hrs, 26/01/90

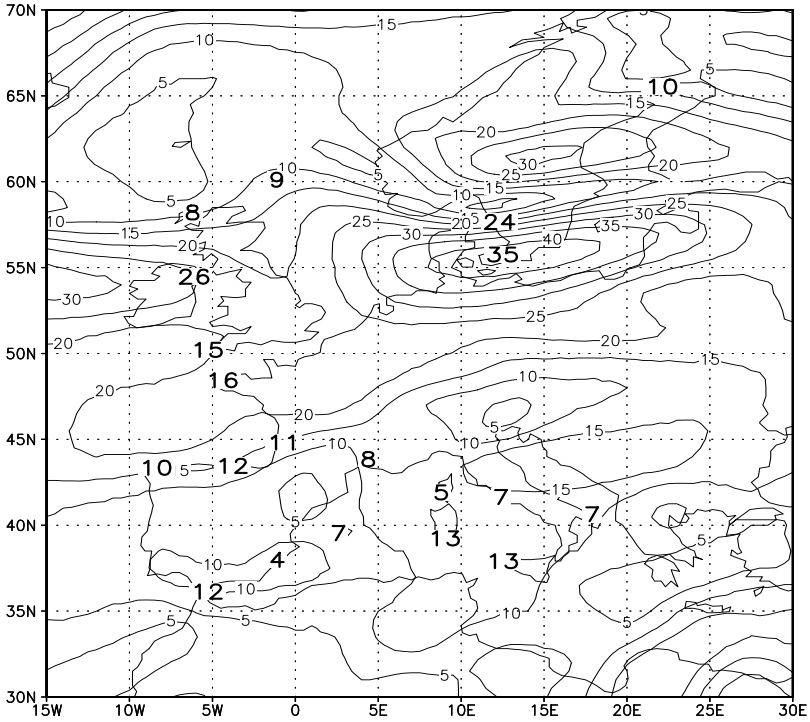

Figure 3.30 Wind speed (m/s) for 12 hrs, 26/01/90

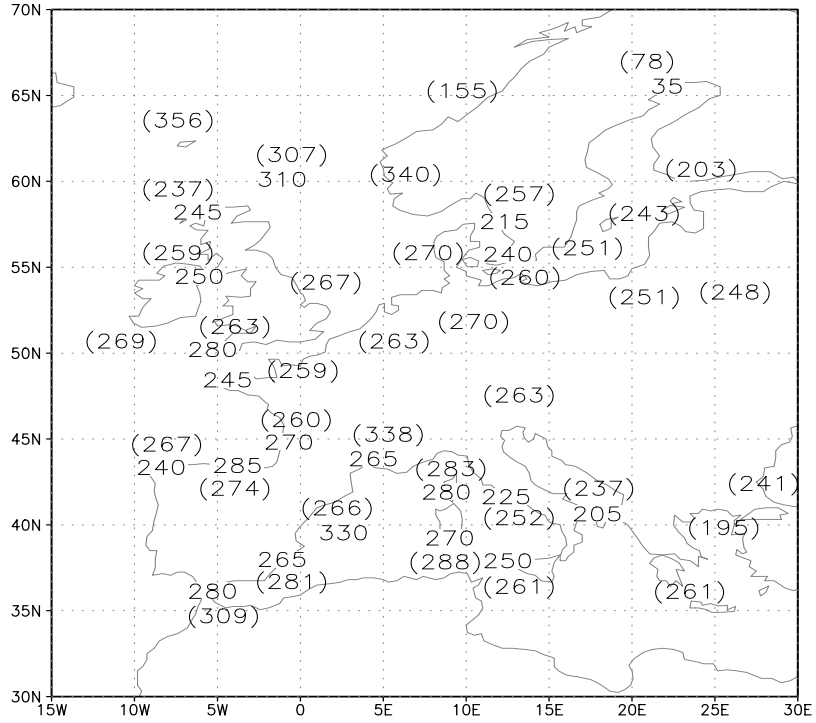

Figure 3.31 Wind direction for 12 hrs, 26/01/90

Winter day, 1 January, 1990

We have noted in the previous example that the radiosonde data appears to suffer from underestimated wind speed and large numbers of missing values in the region of severe storms. We now examine the relationship between the calculated geostrophic wind speed and direction, and the equivalent radiosonde data, during more "normal" conditions in winter and summer. Our first example is a "typical" winter scenario reflecting the relatively calm conditions associated with the establishment of a continental anticyclone, taking three successive 12-hourly time steps beginning at 00 hrs, 1 January, 1990.

00 hrs, 1/1/1990

Figures 3.32 and 3.33 indicate that the geostrophic and radiosonde wind speed and direction compare much more favourably during the low wind speed regime associated with anticyclonic weather. A notable exeception is Italy, which appears to have inaccurate wind speed and direction from the radiosonde data.

12 hrs, 1/1/1990

Comparisons remain good twelve hours later, although the radiosonde data for southern Italy still appears to have problems (Figures 3.34 and 3.35).

00 hrs, 2/1/1990

Again, the overall comparison is good, but parts of Italy still have problematic radiosonde data (Figures 3.36 and 3.37).

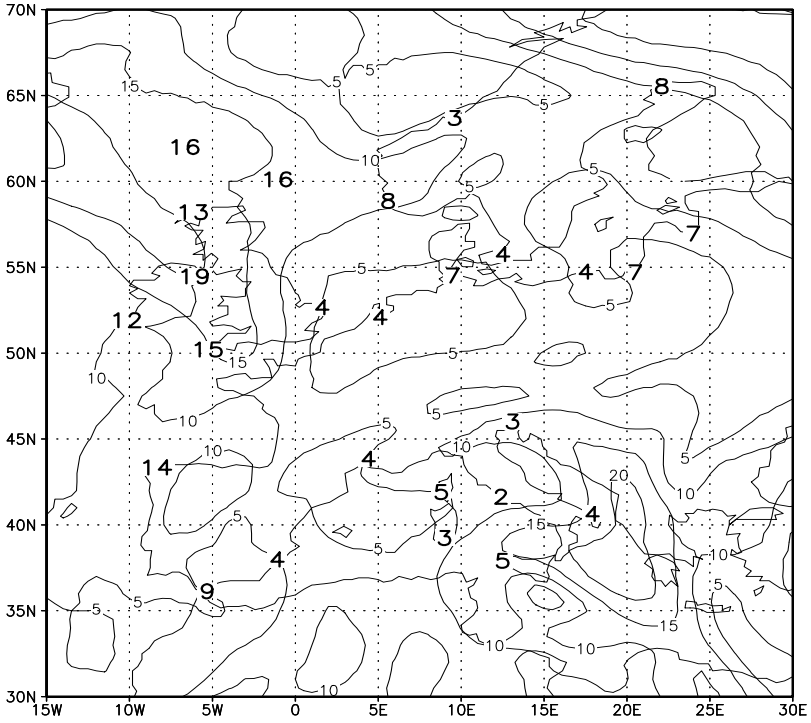

Figure 3.32 Wind speed (m/s) for 00 hrs, 01/01/90

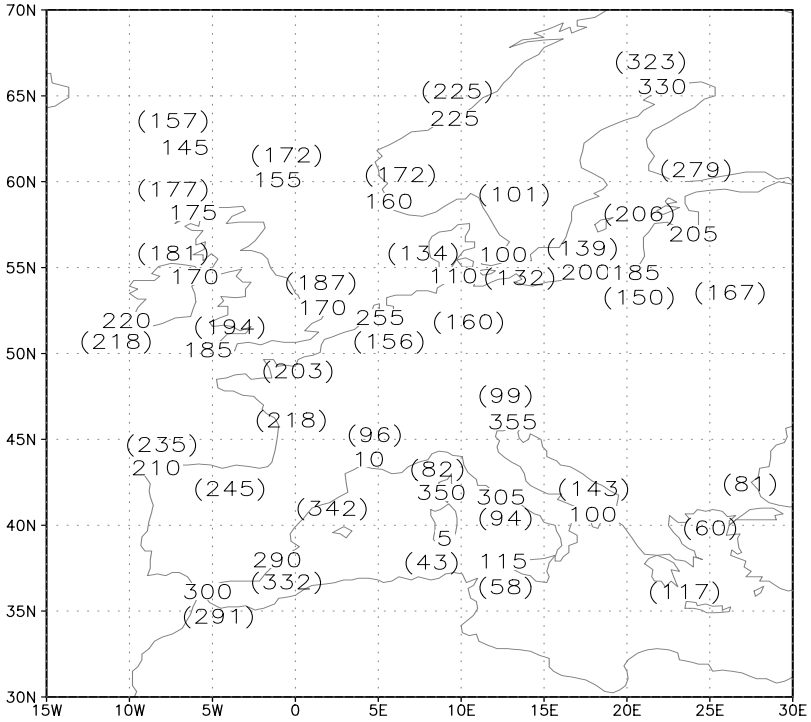

Figure 3.33 Wind direction for 00 hrs, 01/01/90

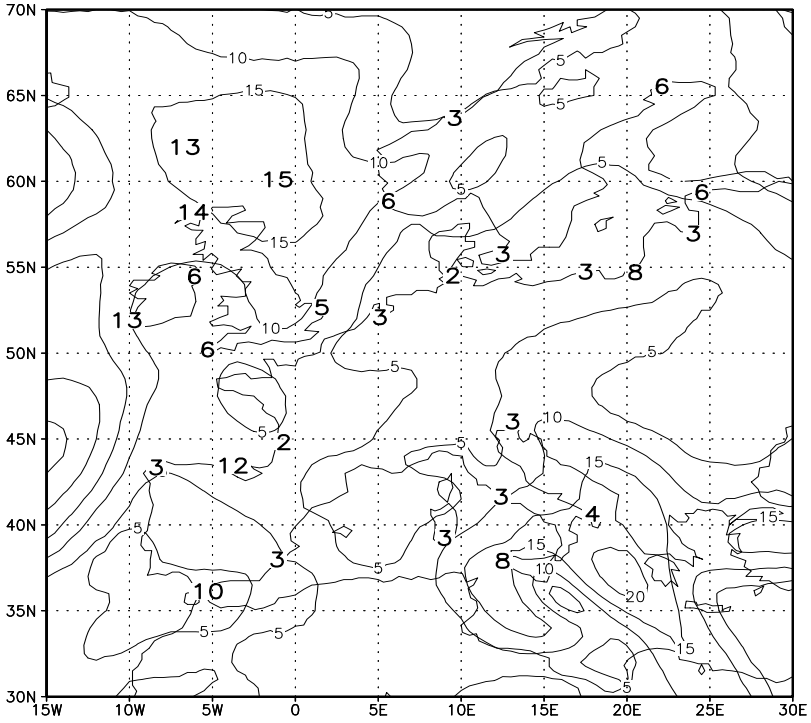

Figure 3.34 Wind speed (m/s) for 12 hrs, 01/01/90

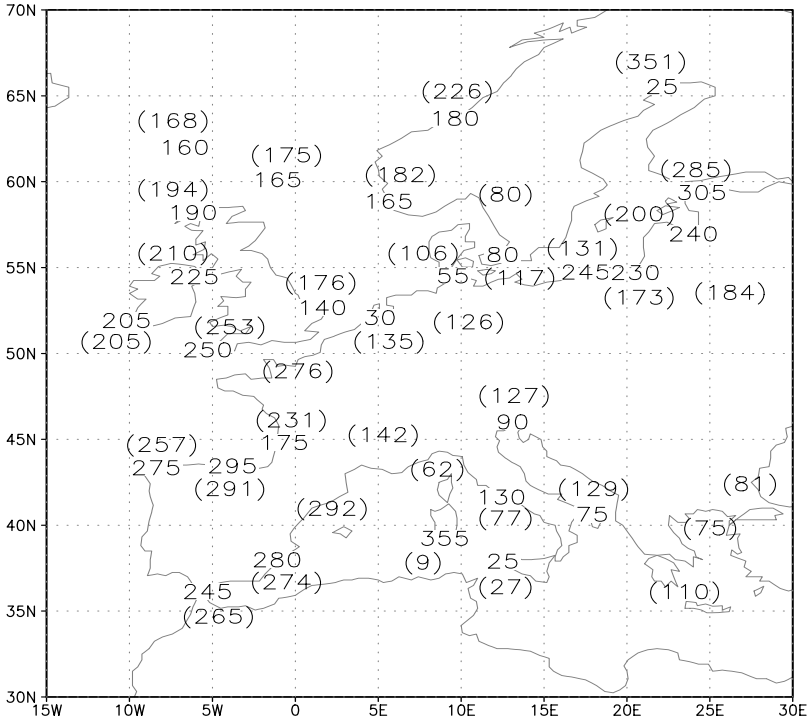

Figure 3.35 Wind direction for 12 hrs, 01/01/90

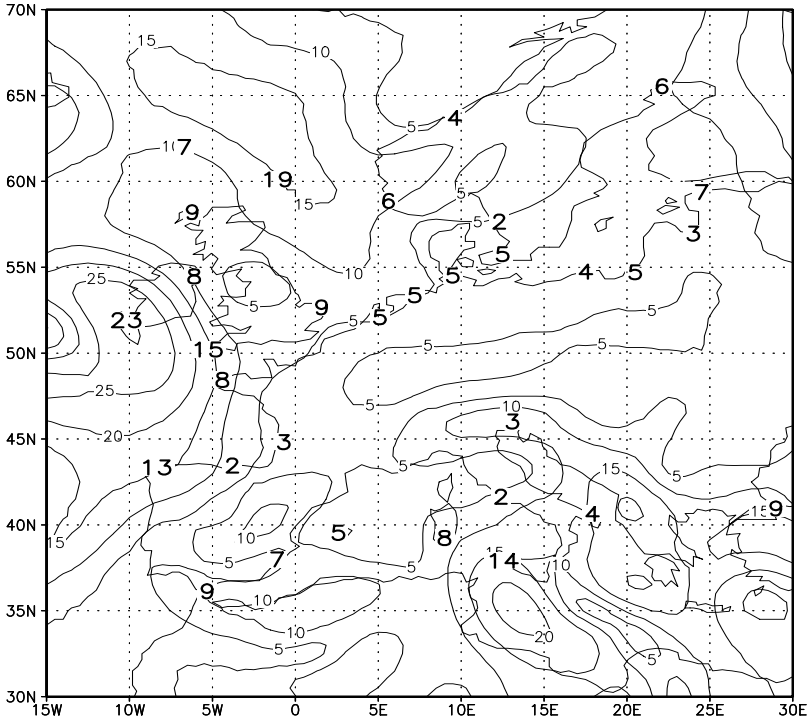

Figure 3.36 Wind speed (m/s) for 00 hrs, 02/01/90

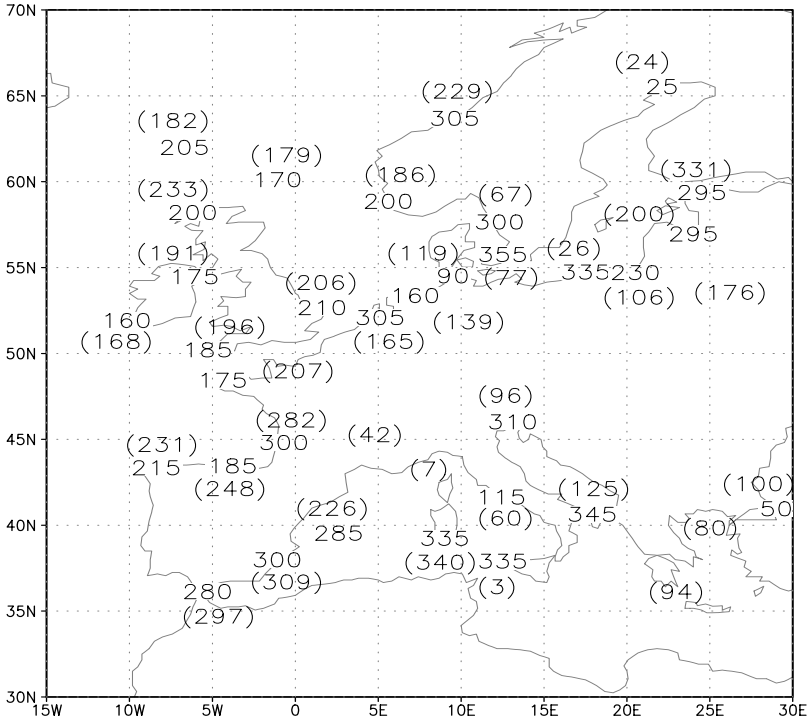

Figure 3.37 Wind direction for 00 hrs, 02/01/90

Summer day, 24 June, 1990

This example shows typically slack summer circulation over Europe.

As might be expected under conditions of low windiness, there is generally good agreement between the geostrophic and observed wind speed and direction throughout the region over all three timesteps (Figures 3.38 to 3.43). Again, southern Italy appears to have incorrect estimates of wind direction from the radiosonde.

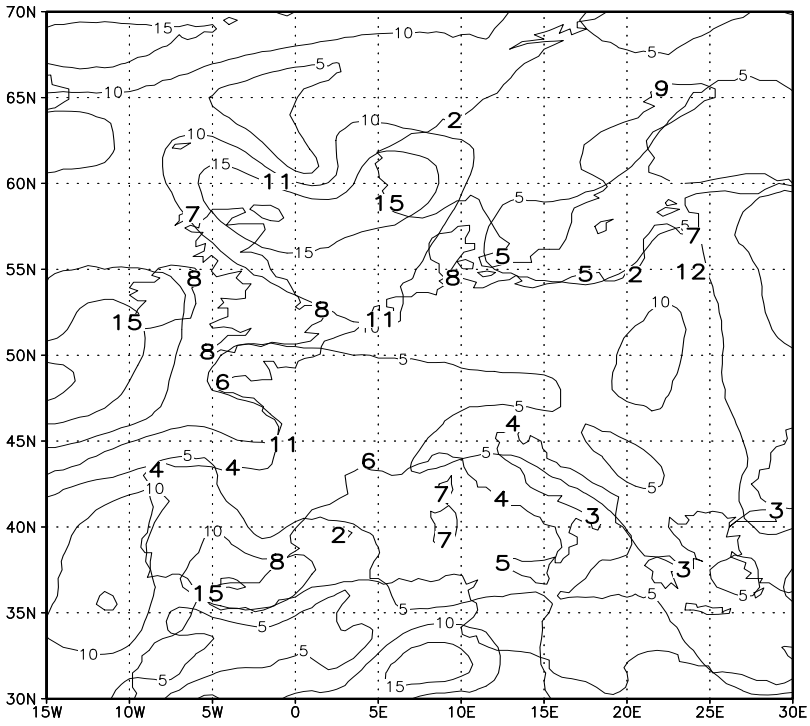

Figure 3.38 Wind speed (m/s) for 00 hrs, 24/06/90

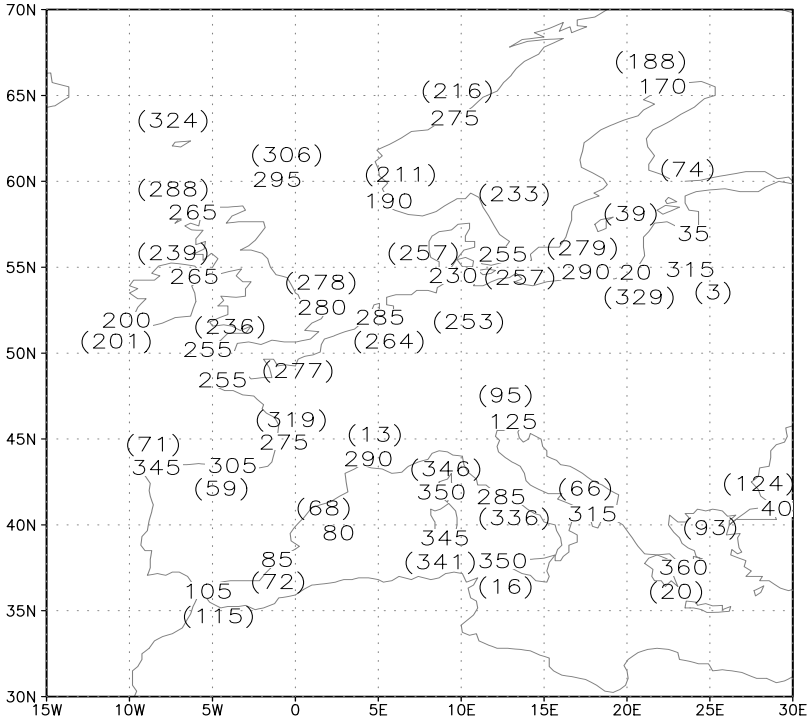

Figure 3.39 Wind direction for 00 hrs, 24/06/90

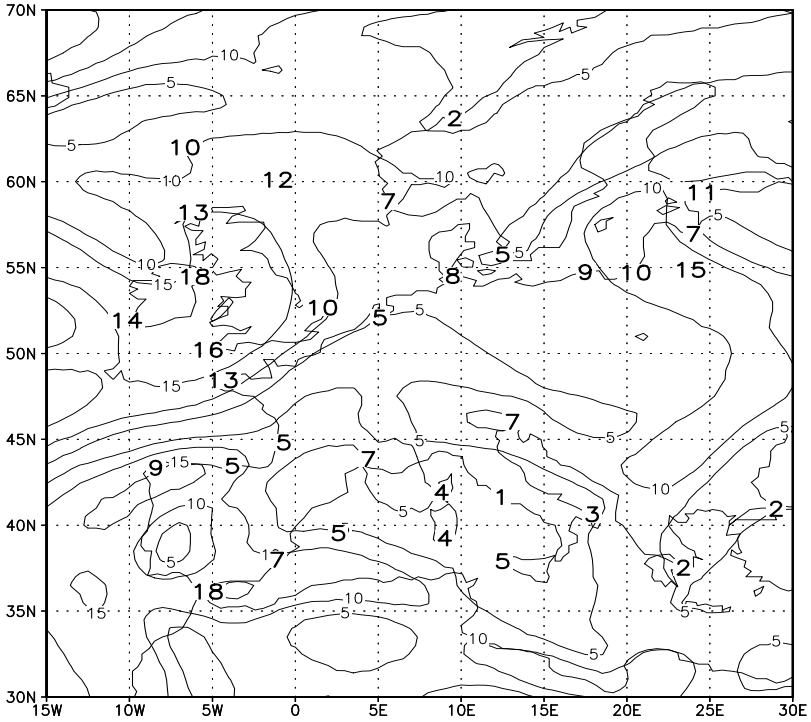

Figure 3.40 Wind speed (m/s) for 12 hrs, 24/06/90

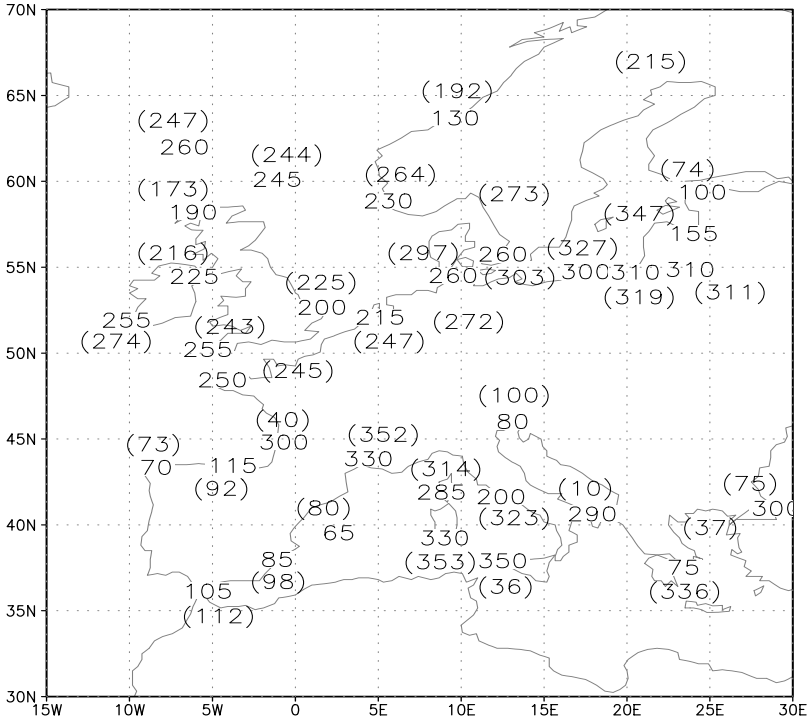

Figure 3.41 Wind direction for 12 hrs, 24/06/90

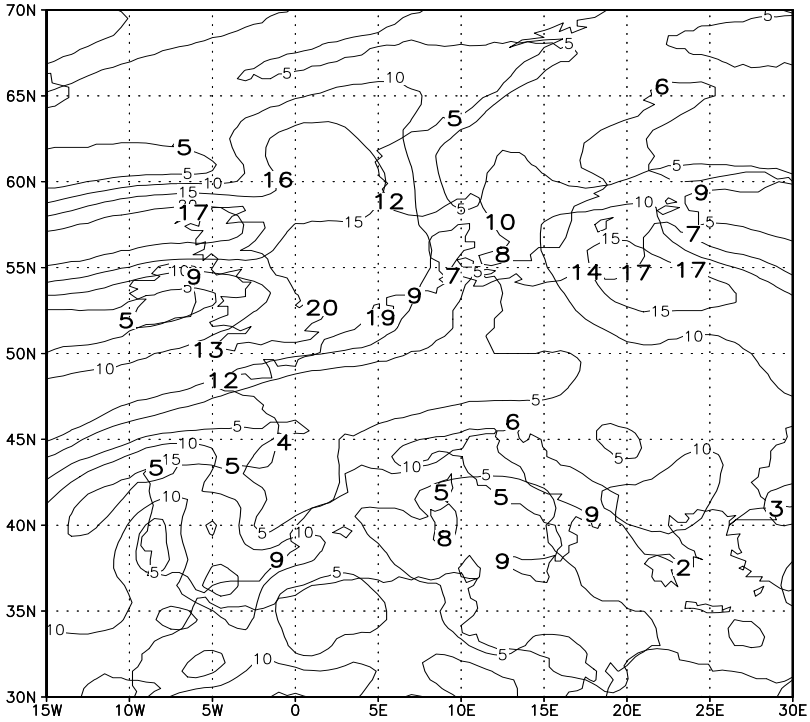

Figure 3.42 Wind speed (m/s) for 00 hrs, 25/06/90

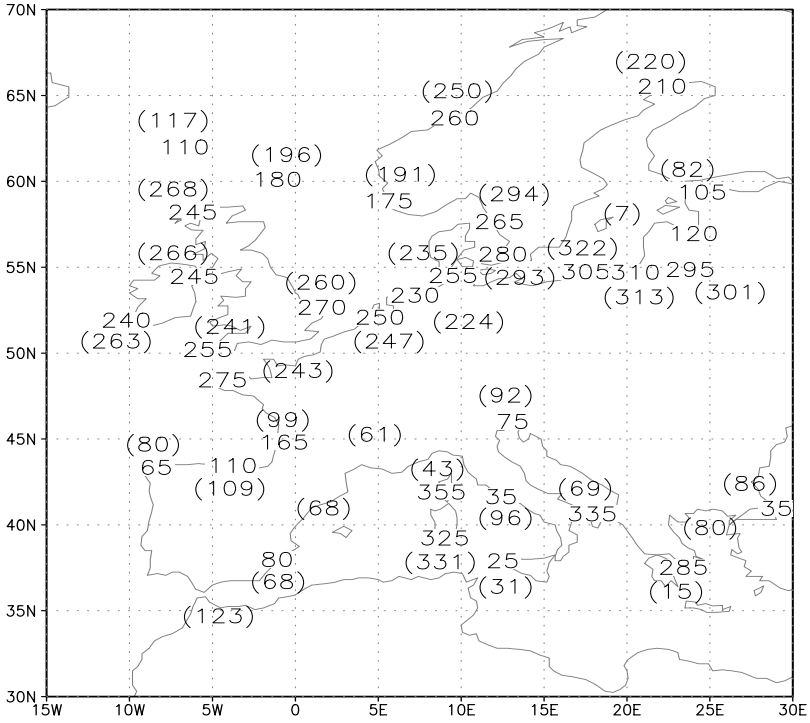

Figure 3.43 Wind direction for 00 hrs, 25/06/90

Winter day, 1 January 1997

We take a final example for a "normal" winter day from 1997. This is because there are fewer missing values in the later years of radiosonde ascents and it gives a more complete picture of the performance of the geostrophic approximation over the Mediterranean.

The overall correspondence between the observed wind speed and direction and the geostrophic values in Figures 3.44 to 3.49 is good. There are very few inconsistencies. The maps demonstrate that the calculated geostrophic wind field is valid for the Mediterranean.

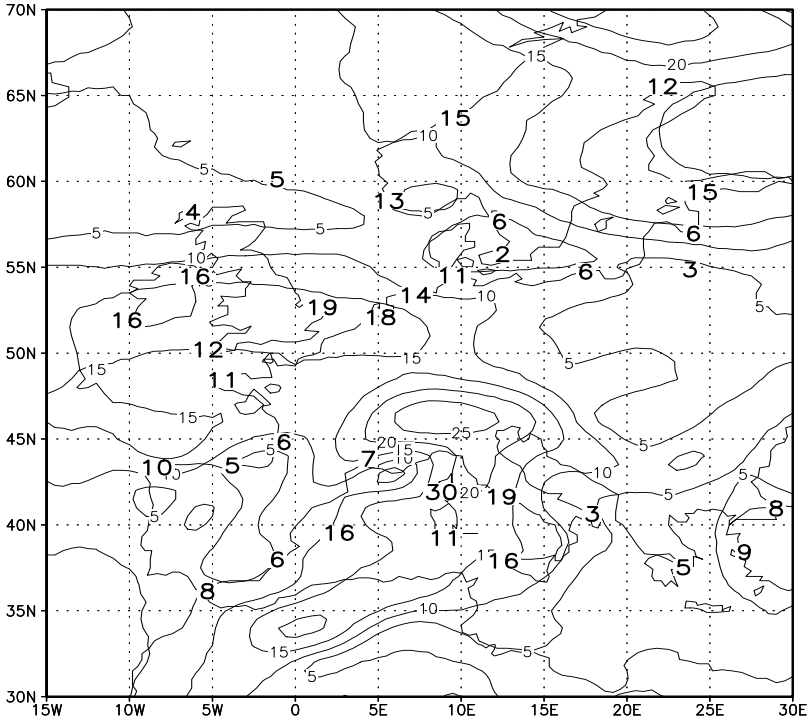

Figure 3.44 Wind speed (m/s) for 00 hrs, 01/01/97

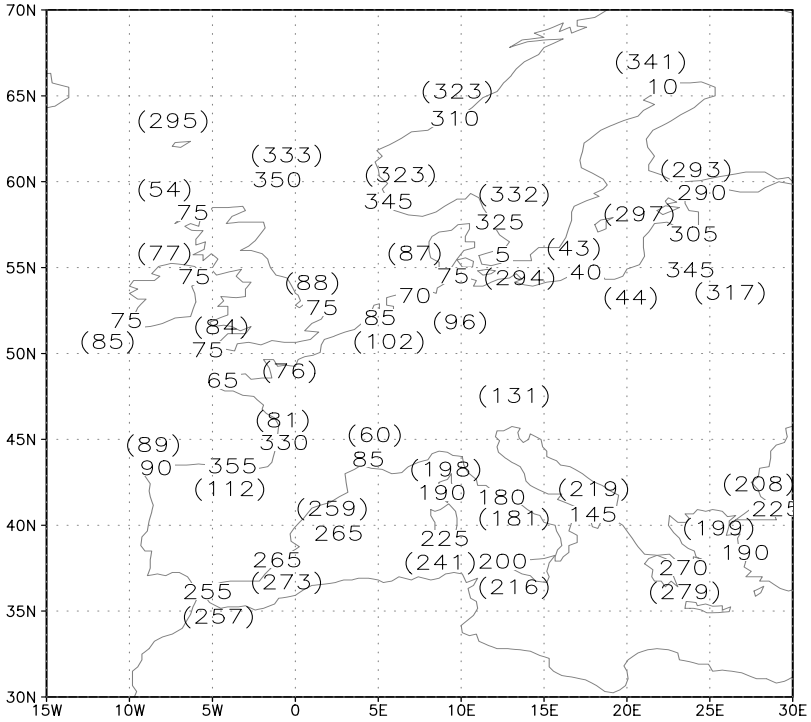

Figure 3.45 Wind direction for 00 hrs, 01/01/97

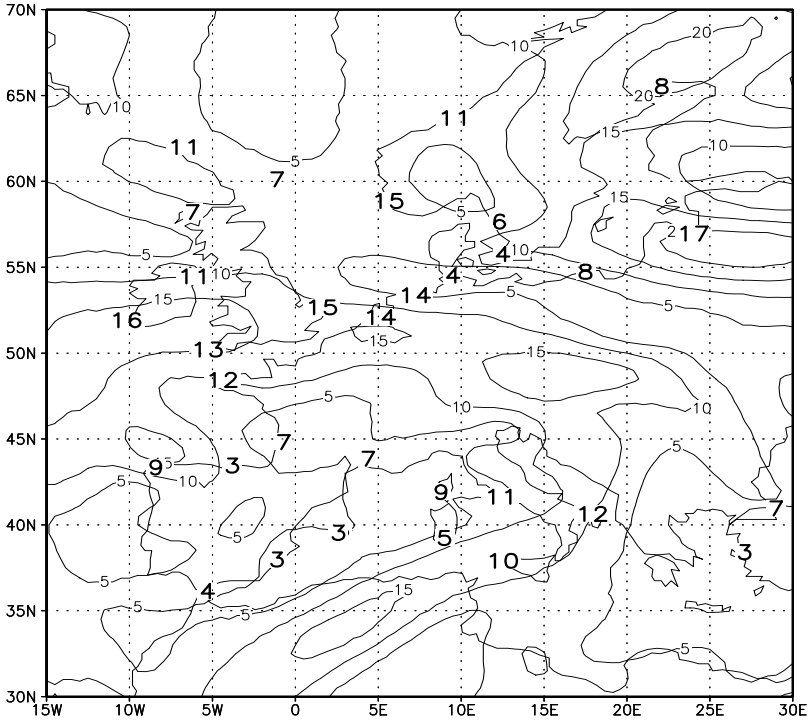

Figure 3.46 Wind speed (m/s) for 12 hrs, 01/01/97

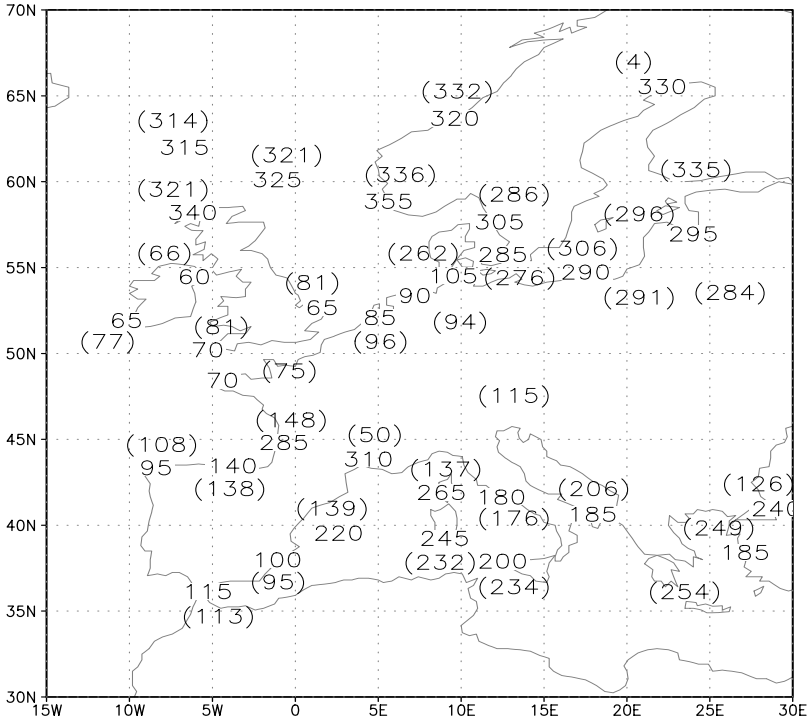

Figure 3.47 Wind direction for 12 hrs, 01/01/97

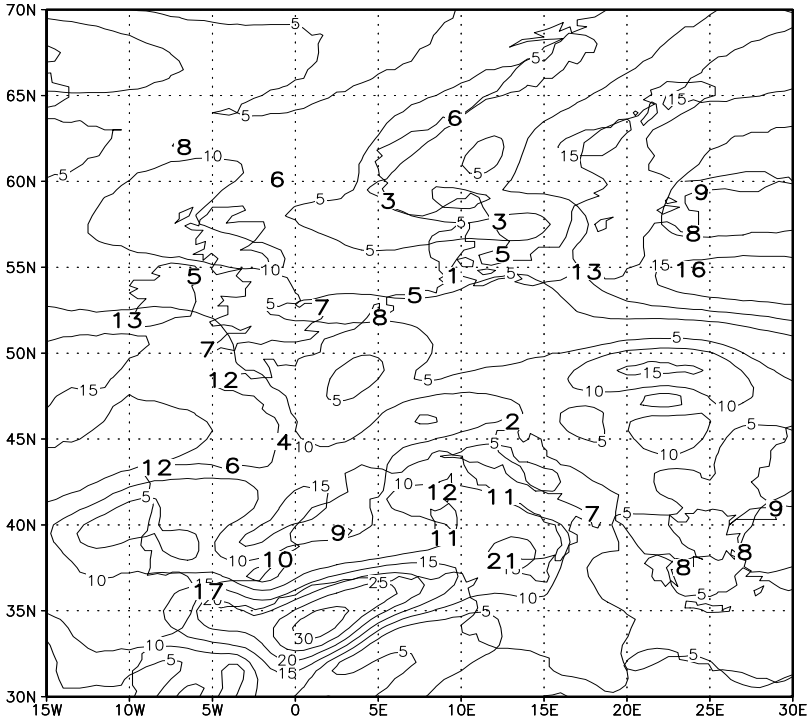

Figure 3.48 Wind speed (m/s) for 00 hrs, 02/01/97

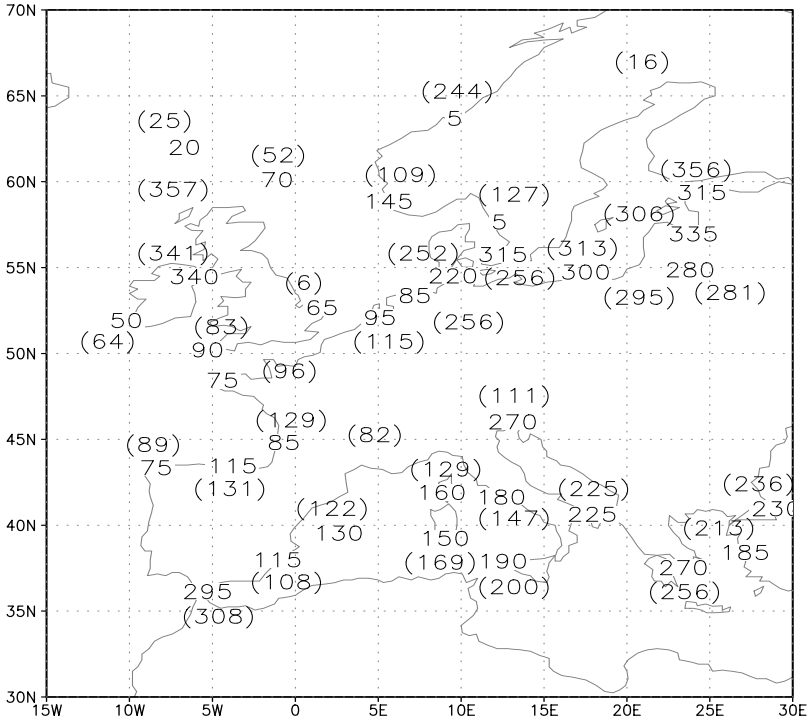

Figure 3.49 Wind direction for 00 hrs, 02/01/97

3.7.3 Comparison of statistics from radiosonde and geostrophic wind data for 1990 and 1997

The examples shown above illustrate qualitatively a fairly good agreement between the geostrophic wind and observations from radiosondes at the first atmospheric levels where friction has little effect on flow. We now extend the study by performing a quantitative comparison. Because of the numerical difficulties in comparing wind directions oscillating between 350 to 10 degrees, we restrict the analysis to wind speeds. We present summary results for all radiosonde ascents from 37 stations during the years 1990 and 1997. The time interval is 12-hourly to accommodate those stations not taking measurements at 6-hourly intervals.

Table 3.5 shows the analysis for the 1990 data. The column headings are:

- id a station identification number related to the numbers in Figure 3.25. The number is preceded by A (Atlantic), B (Baltic), or M (Mediterranean) depending on the sub-basin in which the station is located.
- r the correlation coefficient between the radiosonde and geostrophic wind speeds
- rmse root mean square error
- miss % percentage of missing values in the radiosonde data
- rng ra the range of the radiosonde data (absolute vale of maximum – minimum)
- rng ge the range of the geostrophic wind speeds
- std ra the standard deviation of the radiosonde data
- std ge the standard deviation of the geostrophic wind speeds
- ave ra the mean of the radiosonde data
- ave ge the mean of the geostrophic wind speeds.

Station 32 had no observations in 1990. The shaded rows in Table 3.5 indicate that these radiosonde stations are giving suspect observations. This is evidenced by one or more of the following:

- anomalously low correlation with geostrophic wind speeds,
- anomalously high rmse,
- anomalously large range,
- anomalies in the mean and/or standard deviation.

Only rows where it is evident that the radiosonde data are in error have been highlighted. For example, for Station 2, the range of 451.7 m/s is clearly in error. There are other rows where there may be problems but the cause is less clear cut. Generally, the summary statistics for 1990 indicate a good relationship between the geostrophic wind and the observed wind from the radiosonde. The last row in Table 3.5 gives the average of the various parameters (excluding the suspect rows). The rows in Table 3.5 are organised by sub-basin to facilitate examination of spatially systematic errors in the data. There are no obviously suspect radiosonde stations in the Atlantic region, four in the Mediterranean, and four (half the stations) in the Baltic.

The equivalent data for 1997 are shown in Table 3.6. The Atlantic has acquired one suspect radiosonde station, and the Baltic has none, an impressive improvement on the 1990 tally. The Mediterranean, on the other hand, still has four suspect rediosonde stations, three of which were present in the 1990 tally (the remaining one had no data in 1990). This apparently persistent failure in instrumentation for 25% of the Mediterranean radiosonde stations requires further detailed examination and possibly remedial

measures such as a training programme sponsored by the WMO.

There is little difference between the summary data for 1990 and 1997, other than that the percentage of missing values has fallen with time.

Although the validation works well, a somewhat surprising result is that the variance and means are slightly higher in both years for the geostrophic wind speeds compared with the radiosonde data. This is the opposite of what would be expected, since the calculation of the geostrophic wind involves an element of spatial smoothing generally assumed to provide less variable and lower estimates of wind speed than would be obtained from measurements in situ. The results also provide independent confirmation of the validity of the interpolation of the pressure data.

Table 3.5 Comparative wind speed statistics for 1990

id	r	rmse	miss %	rng ra	rng ge	std ra	std ge	ave ra	ave ge
A3	0.85	3.1	29	35.5	34.4	5.9	6.4	10.6	11.5
A5	0.76	3.1	21.5	27.3	29.1	4.8	5.4	7.6	8.2
A6	0.79	3.1	42.5	26.8	38.4	5	6.2	9.2	10.4
A8	0.87	2.7	66.7	27.3	35	5.7	6.9	9.8	10.5
A9	0.89	3	9.6	31.9	33.1	6.6	6.9	11.6	11.9
A12	0.92	2.5	11	34.5	39.8	6.5	6.9	11.5	12.1
A20	0.9	2.7	9	32.4	39.2	6.2	7	10.3	11
A21	0.73	4.4	22.2	37	33.3	6.4	6.6	9.8	11
A22	0.84	3.2	24.4	31.9	41.6	5.8	7.2	10.3	12.3
A25	0.8	3.3	15.1	31.9	38.7	5.6	6.7	8.8	11
A28	0.69	3.6	29.9	31.4	35.3	4.9	6	6.9	8.9
A33	0.9	2.7	8.6	36.5	44.8	6.2	6.8	11.6	11.6
A34	0.89	2.7	11	37.6	46.2	6.1	7	10.8	11.4
A35	0.91	2.9	10.7	35.5	38.1	7	8	12.3	13.2
A36	0.89	3	16.8	32.4	37.2	6.4	6.9	11.5	12.3
A37	0.9	3	15.2	38.1	46.8	6.9	7.5	12.3	12.9
Aave	**0.85**	**3.1**	**21.5**	**33.0**	**38.2**	**6.0**	**6.8**	**10.3**	**11.3**
B1	0.87	3	12.2	46.8	41.5	6.1	6.6	10.3	11
B2	0.19	18.6	18.1	451.7	30.9	19	5.7	10.5	9.9
B18	0.87	2.8	10	31.9	36.7	5.7	6.1	10.2	10.6
B19	0.31	13.1	18.4	300.9	33.4	13.8	5.8	10.5	10.3
B23	0.89	2.8	18.8	30.9	32.9	6.2	6.5	11.3	11.1
B24	0.58	6.8	34.9	106	33.5	8.4	6.5	11.1	10.8
B29	0.8	3.7	56.7	35	32.4	6.3	6.4	10.9	10.5
B30	0.55	5.7	31	108	30	6.8	5.2	8.5	9
Bave	**0.86**	**3.1**	**24.4**	**36.2**	**35.9**	**6.1**	**6.4**	**10.7**	**10.8**
M4	0.39	2.2	34	13.4	32.3	2.4	4.4	4.3	5.5
M7	0.71	3.6	28.8	26.2	29.8	5.2	5.8	8.6	8.9
M10	0.74	3.3	5.9	24.7	28.4	4.9	4.8	9.1	8.5
M11	0.7	2.8	29	23.7	21.7	3.9	4.1	6.2	7.1
M13	0.46	5.2	21.1	100.3	32.9	5.9	4.8	6.9	6.6
M14	0.76	2.9	21.4	29.3	30.7	4.5	5.1	6.8	7.2
M15	0.52	3.1	21.4	25.2	28.4	3.6	4.5	5	5.8
M16	0.72	3.4	26	29.8	38.5	4.8	5.2	7	7.3
M17	0.26	3.6	18.9	54.5	33	3.7	5.4	3.8	8
M26	0.69	2.5	9	19	27.9	3.5	4.5	5.2	6.7
M27	0.71	2.7	12.7	20.6	26.6	3.9	3.6	5.6	5.6
M31	0.24	8.9	54	158.4	25.7	9.2	5.8	6.8	10
M32									
Mave	**0.69**	**3.0**	**19.3**	**24.8**	**29.0**	**4.3**	**4.7**	**6.7**	**7.1**

Table 3.6 Comparative wind speed statistics for 1997

id	r	rmse	miss %	rng ra	rng ge	std ra	std ge	ave ra	ave ge
A3	0.86	3.1	16.8	35	36.2	6.1	6.7	11.2	11.9
A5	0.74	3.1	11.1	25.2	27.9	4.6	5.2	7.7	8.2
A6	0.5	8.8	12.3	216.6	36.1	10.2	6.6	10.3	10.6
A8	0.82	3.3	10.5	35	32.8	5.8	6.2	9.8	10.4
A9	0.86	3.1	10.1	30.4	34.4	6.1	6.4	10.5	10.9
A12	0.9	2.7	11.4	34	32.6	6	6.6	11	11.5
A20	0.87	2.8	7.1	29.8	32.7	5.6	6.1	9.5	10.2
A21	0.72	4.6	19.3	37	41.1	6.6	7	9.6	10.9
A22	0.84	3.1	14.1	29.8	40.1	5.9	6.9	10	11.3
A25	0.81	3.4	33.8	31.9	31.5	5.8	6.9	8.6	11.2
A28	0.62	3.8	22.9	32.9	33.1	4.8	5.8	6.5	8.7
A33	0.89	2.8	2.7	36.5	41.6	6.2	6.6	10.9	10.7
A34	0.88	2.7	4.9	32.4	45.6	5.8	6.5	10	10.2
A35	0.89	2.9	2.5	34	41.3	6.4	7.5	10.8	11.9
A36	0.91	2.8	5.3	33.4	42.7	6.7	7.1	12.1	12.3
A37	0.88	3.1	4.4	37.6	40.5	6.7	7.3	11.4	11.9
Aave	**0.83**	**3.2**	**11.8**	**33.0**	**36.9**	**5.9**	**6.6**	**10.0**	**10.8**
B1	0.85	2.9	7.4	27.8	40.1	5.6	6.1	9.7	9.9
B2	0.76	3.4	16.4	29.8	44.3	5.2	5.8	8.9	10
B18	0.82	3.1	50.5	26.8	34.6	5.4	6.2	10	10.8
B19	0.85	2.9	53.2	25.7	27.1	5.5	5.9	9.8	10
B23	0.88	2.7	16	36	35.1	5.7	6	10	10.3
B24	0.8	4.3	89.3	30.9	31.3	7.2	7	12.9	13.6
B29	0.8	3.2	21.1	30.9	36.1	5.3	6.1	9.6	9.3
B30	0.76	3.5	26.4	25.7	27.5	5.4	5.8	9.3	9.7
Bave	**0.82**	**3.3**	**35.0**	**29.2**	**34.5**	**5.7**	**6.1**	**10.0**	**10.5**
M4	0.29	4.8	10.5	58.1	30.2	5	4.5	5.6	6.1
M7	0.74	3.8	11.2	44.2	33.5	5.7	6.5	8.6	9.3
M10	0.71	3.1	5.3	25.7	28	4.4	4.6	9.2	7.9
M11	0.7	2.7	35.1	19	24.7	3.8	4.3	6.1	7
M13	0.67	3.5	9.3	28.8	32	4.7	5.5	8.1	7.5
M14	0.76	2.9	17.9	26.2	28.1	4.4	5.2	7.3	7.3
M15	0.54	3.2	9.2	22.6	33.4	3.9	4.8	5.9	6.2
M16	0.73	3.1	17	25.2	26.3	4.5	4.9	7.3	7.5
M17	0.44	2.8	12.9	21.6	34.3	3.1	5.9	3.9	9
M26	0.6	2.8	20	20.6	27.4	3.5	4.6	5.9	6.7
M27	0.66	3.4	20.1	26.8	30.8	4.5	4.6	6.8	6.2
M31	0.49	4.1	2.6	75.6	28.8	4.7	6	6.1	9.7
M32	0.33	3.3	1.4	22.1	30.4	3.5	6	5.5	9.9
Mave	**0.68**	**3.2**	**16.1**	**26.6**	**29.4**	**4.4**	**5.0**	**7.2**	**7.3**

3.7.4 Comparison of seasonal cycles of radiosonde and geostrophic speeds

Figure 3.50 shows the 1990 seasonal pattern of wind speed, from the geostrophic approximation and the radiosonde ascents, for the Atlantic, Baltic, and Mediterranean basins respectively. Monthly averages for each are presented, calculated by averaging for all points within each basin over time and space for the year 1990.

For the Atlantic (Figure 3.50a) there is a good match between the mean monthly wind speeds with the largest discrepancies occurring in the months when the wind speeds are highest. This is either because radiosonde data are inherently unreliable during periods of very high wind speeds, or because the most reliable radiosonde sites are those most affected by missing values during North Atlantic storms, thus biasing the monthly means towards less reliable sites. The Baltic (Figure 3.50b) provides a near-perfect match between the monthly mean wind speeds. The discrepancies noted in the Mediterranean chart (Figure 3.50c) simply reflect the persistent unreliability already noted at certain sites in the

region. At such low mean wind speeds the match should be much closer.

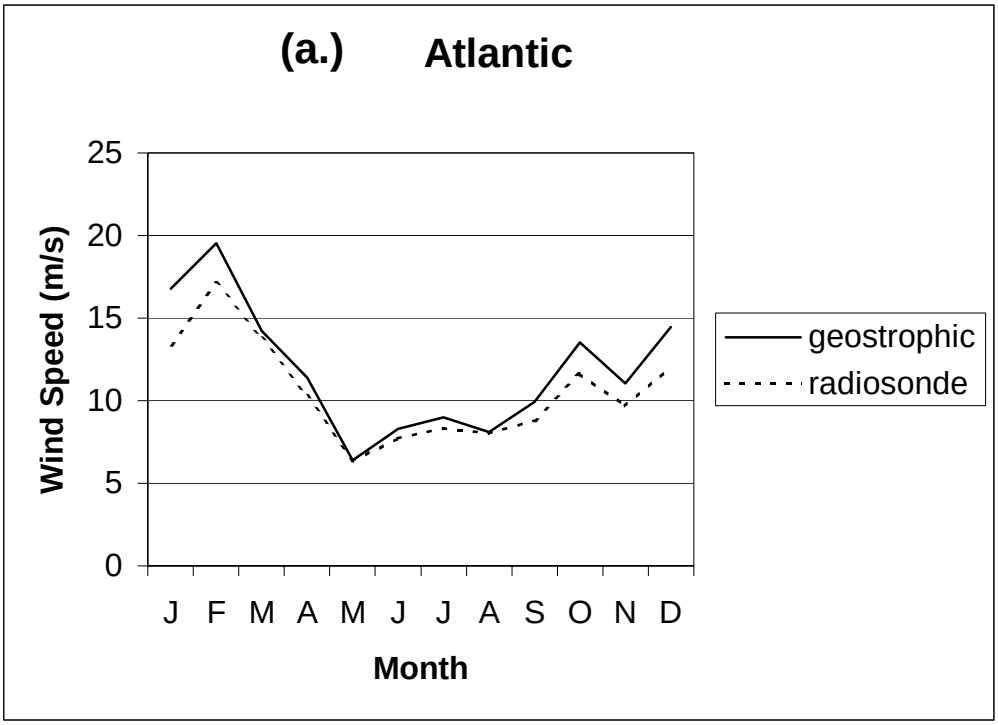

Figure 3.50 Seasonal cycles of wind speed from the Atlantic, Baltic and Mediterranean basins

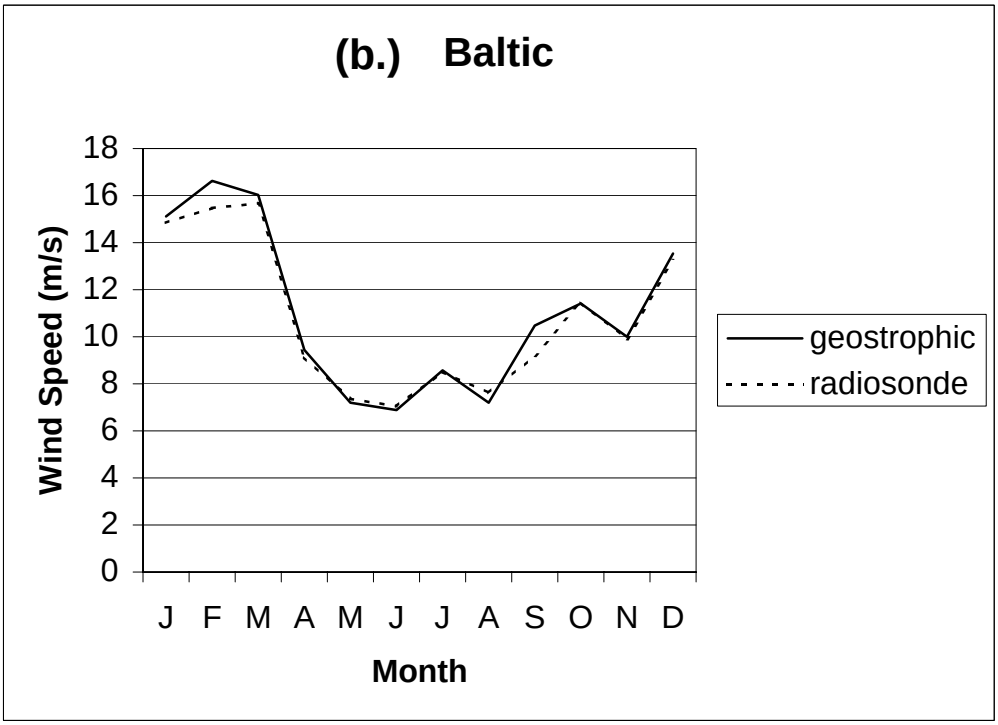

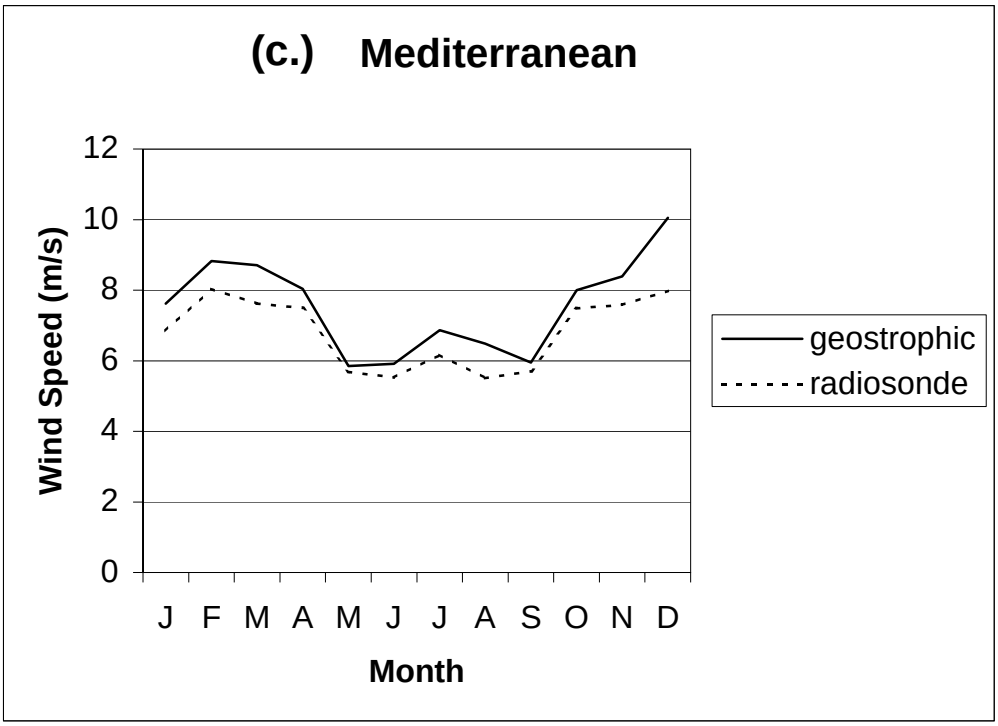

Figure 3.51 Seasonal cycles of wind speed from the Atlantic, Mediterranean and Baltic basins (continued)

3.7.5 Conclusions regarding comparison of POWER geostrophic winds with radiosonde data

Examination of the radiosonde wind data used in POWER reveals many inconsistencies that would make them extremely difficult to use on their own. The Mediterranean appears to be particularly prone to suspect radiosonde data, whereas the Atlantic, and latterly the Baltic, appears to give reliable information. Used to validate geostrophic flow, however, these data are extremely valuable. It is reasonable to assume that, even if they contain systematic errors, the geostrophic data are spatially consistent. This enables us to readily identify suspect radiosonde data, such as the Italian observations for 1 January 1990, and use the remainder for validation.

Given that the radiosonde data are point information, and the geostrophic winds are derived from gridded data with an element of spatial averaging, the results of the validation are remarkably good. The maps and tables provided in this report indicate that the geostrophic wind and direction calculated from the interpolated pressure data are an excellent representation of frictionless flow between 600 and 900 m over the ocean and immediate coastal regions of Europe, including the Mediterranean and the Baltic Sea.

3.8 Results

Figure 3.52 presents a plot of the distribution of mean annual geostrophic wind speeds calculated from the NCEP atmospheric pressure data in the period 1985 - 1997.

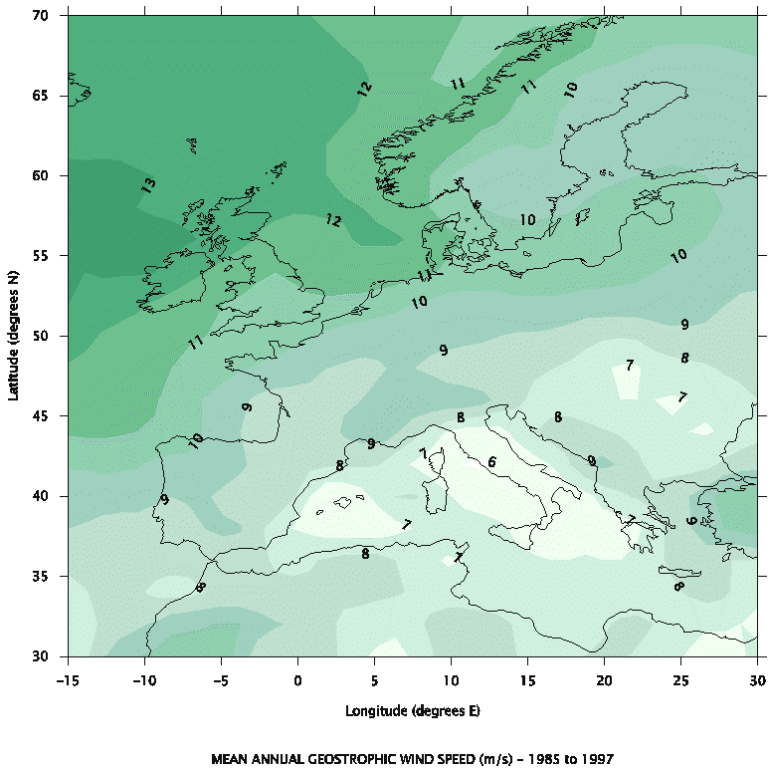

Figure 3.52 Calculated mean annual geostrophic wind speeds (m s^{-1}) – 1985 to 1997

3.9 Conclusions

This chapter has demonstrated that geostrophic winds are an accurate representation of friction-free wind over the ocean and coastal areas:

- The geostrophic wind speed and direction are consistent with frictionless flow from radiosonde observations at coastal stations,
- Where radiosonde data are unreliable, the geostrophic wind speed and direction data provide a spatially consistent alternative,
- Patterns of geostrophic flow are consistent with the surface wind field.

Therefore, the geostrophic wind is suitable for used in the POWER project as the basis for calculating the surface wind using WAsP. This procedure is described in Chapter 4.

3.10 References for Chapter 3

James, I.N. (1994): Introduction to Circulating Atmospheres. Cambridge University Press, Cambridge.

Kalnay, E. et al. (1996): The NCEP/NCAR 40-year reanalysis project. Bull. Amer. Meteor. Soc. 77, 437-471.

McIlveen, R. (1992): Fundamentals of Weather and Climate. Chapman & Hall, London. 497 pp.

Press, W.H. (1992) Numerical Recipes in FORTRAN: The Art of Scientific Computing. Second Edition. Cambridge. 963 pp.

Watson, D.F. (1992) Contouring. A Guide to The Analysis and Display of Spatial Data. Pergamon. 321 pp